Received 10 January 2024; revised 26 January 2024; accepted 27 January 2024. Date of publication 30 January 2024; date of current version 16 February 2024.

Digital Object Identifier 10.1109/OJCOMS.2024.3360288

Max-Min Throughput Optimization in WPCNs: A Hybrid Active/Passive IRS-Assisted Scheme

IQRA HAMEED AND INSOO KOO (Member, IEEE)

Department of Electrical, Electronic and Computer Engineering, University of Ulsan, Ulsan 44610, South Korea

CORRESPONDING AUTHOR: I. KOO (e-mail: iskoo@ulsan.ac.kr)

This work was supported in part by the National Research Foundation of Korea through the Korean Government Ministry of Science and ICT (MSIT) under Grant NRF-2021R1A2B5B01001721, and in part by the Regional Innovation Strategy (RIS) through the National Research Foundation of Korea (NRF) funded by the Ministry of Education (MOE) under Grant 2021RIS-003.

ABSTRACT The integration of wireless powered communication network (WPCNs) with intelligent reflecting surface (IRS) technology has emerged as a promising solution for enhancing the energy and spectral efficiency of the network. Recent studies have explored the benefits of active and passive reflecting element surfaces in various networks. However, most existing works on IRS-assisted WPCNs mainly focus on comparing an active IRS to single/multiple IRSs or to a hybrid IRS comprising active and passive elements on the same surface. In this paper, we explore a hybrid, active and passive IRS-assisted WPCN which can significantly improve network capacity. By introducing a distributed pair of active and passive IRSs, signal amplification and multiple reflection links can boost the wireless link capacity. To enhance network performance, this new framework utilizes both active and passive IRS elements to optimize wireless energy transfer (WET) on the downlink and wireless information transfer (WIT) on the uplink. However, designing a joint deployment of active and passive IRS elements becomes more challenging due to the joint operations of downlink WET and uplink WIT in WPCNs. To address the complexity of the non-convex optimization problem associated with the hybrid IRS-aided architecture, we use a systematic divide-and-conquer methodology. This decomposes the main problem into three interconnected sub-problems that are solved sequentially using sophisticated techniques. Furthermore, the study examines two practical deployment scenarios for active and passive IRS elements, namely 'Hybrid Case-1' (where active IRS is placed near the hybrid access point (H-AP) and passive IRS is placed near wireless devices) and 'Hybrid Case-2' (where active IRS is placed near wireless devices and passive IRS is placed near the H-AP). Extensive simulations and numerical analysis demonstrate the superiority of our proposed hybrid IRS-based framework over single active IRS and conventional double passive IRSs-assisted network, making it a promising and compelling solution for practical WPCN deployments, ensuring enhanced network performance and throughput fairness in wireless power and communications technologies.

INDEX TERMS Hybrid active and passive intelligent reflecting surface (IRS), throughput fairness, wireless energy transfer (WET), wireless information transfer (WIT), non-convex optimization, semi-definite program (SDP), semi-definite relaxation (SDR), successive convex approximation (SCA), lagrangian optimization.

I. INTRODUCTION

THE INTERNET of Things (IoT) has emerged as a transformative technology that connects billions of smart devices, enabling data-driven decision-making, automation, and improved efficiency across various industries [1], [2], [3]. However, the rapid growth of IoT devices brings forth significant challenges, particularly concerning power supplies and connectivity. Traditional battery-powered IoT devices often suffer from limited lifespans and environmental concerns, requiring frequent maintenance due to battery disposal. To overcome these challenges, a revolutionary concept known as the wireless

powered communication network (WPCN) in the IoT has emerged, promising to unlock new horizons for energy-efficient and seamless IoT ecosystems [4], [5]. A WPCN in the IoT combines the principles of wireless power transfer and wireless communications to create a paradigm where IoT devices harvest energy from a radio frequency signal transmitted by an energy provider, eliminating the need for traditional batteries. This integration of power and data transmission not only ensures continuous and sustainable operation of IoT devices but also opens up new possibilities for IoT applications in various domains [2].

In a conventional WPCN architecture, there is a hybrid access point (H-AP) that plays a central role in coordinating multiple wireless devices for wireless energy transfer (WET) on downlink and wireless information transfer (WIT) on uplink. The H-AP serves as the power transmitter, generating and transmitting wireless power to devices in the network. In the context of WPCNs, a harvest-then-transmit protocol is considered [6], which means that the wireless devices within the network do not have their own battery sources. Instead, they rely on harvesting energy from the H-AP to power their operation. The devices harvest and store the wireless power transmitted by the H-AP and utilize the harvested energy to transmit information to the H-AP on uplink, eliminating the need for traditional batteries, and reducing maintenance. Efficient performance of a WPCN relies on the joint design of energy and information transmission. It is essential to find the optimal allocation of time for both WET and WIT to achieve the required quality of service (QoS) in the network. The allocation of time for energy transfer and information transmission directly impacts the energy efficiency and throughput of the WPCN. Moreover, wireless power transfer also faces challenges when devices are at a considerable distance from the H-AP because the transmitted energy suffers from more significant path loss and attenuation. As a result, a distant device receives considerably less energy, making it more challenging for the device to sustain operations and transmit data on uplink (UL). This is called *doubly-near-far* problem, which is a significant throughput fairness issue that arises in WPCNs, leading to imbalanced energy harvesting and data transmission capabilities depending upon the channel conditions between the H-AP and the devices [6], [7]. To enhance energy harvesting (EH) efficiency and extend the distance of information transmission in WPCNs, researchers have proposed various technologies. Some of these technologies include relay cooperation and massive multiple-input multiple-output (MIMO) technology, among others. However, practical implementations of these technologies come with challenges related to power consumption, hardware cost, and signal processing complexity [8].

Recently, intelligent reflecting surface (IRS)-assisted wireless networks have emerged as a promising solution to address the increasing demands of mobile and communication devices. By utilizing a smart radio environment, the IRS, also known as the reconfigurable intelligent surface (RIS), can enhance the energy and spectral efficiency of networks. These surfaces consist of multiple reflecting elements that can independently reconfigure their reflecting properties, enabling better control over signal propagation, and enhancing network performance [9], [10], [11], [12], [13]. By optimizing signal reflections and controlling signal paths, IRSs can mitigate signal attenuation and enhance coverage, leading to improved signal quality and increased data rates for devices. Moreover, an IRS can help manage interference, optimize resource allocation, and improve overall network performance. The concept behind IRSs is to deploy reflective surfaces with the ability to control the amplitude or phase of incident or reflected signals. By intelligently adjusting the properties of these surfaces, IRSs can effectively combat fading environment impairments and interference challenges [12], [14], [15], [16]. With advancements in metasurfaces and micro-electromechanical systems (MEMS), it is now possible to reconfigure IRS elements in real time using controllable phase shifters [17]. This dynamic reconfiguration allows adaptability to various communication scenarios and environmental conditions. For example, several authors deployed the single passive IRS to improve network performance [5], [8], [13], [18], [19]. Shi et al. discussed how deploying a single passive IRS in a secure WPCN can significantly enhance downlink energy transfer and uplink information transmission efficiency [8]. They maximized the secrecy throughput of all devices while jointly optimizing the phase shift matrices of the passive IRS and time allocations on downlink and uplink. Zheng et al. exploited the IRS to enhance energy and spectral efficiency by maximizing the minimum throughput in cooperative WPCNs [18]. Their proposed IRS-assisted cooperation method achieved 91.85% higher throughput than cooperation without an IRS. Hameed et al. combined the single passive IRS with a cognitive radio (CR)-enabled WPCN and studied the effectiveness of a passive IRS on the sum throughput of cognitive users in the presence of potential primary users [13]. In [16], the author highlighted the benefits of the joint exploitation of the IRS technology within the context of non-orthogonal multiple access (NOMA)-enabled simultaneous wireless information and power transfer (SWIPT) IoT networks. However, these single-IRS deployments have limitations in fully optimizing the IRS benefits for communication performance. The single-IRS deployment strategies mentioned earlier align with a theoretical finding, indicating that an IRS should be placed near the transmitter or receiver to minimize severe path loss over the two links involving the IRS, its assisted base station (BS), and the devices [15]. So, a single-IRS deployment's limitations include limited coverage, potential blockage issues, constrained passive beamforming gain, and limited spatial multiplexing gain due to correlated channels [20].

To overcome the limitations of single-IRS systems, researchers are exploring advanced strategies like multiple IRS deployments, cooperation, dynamic control, and hybrid beamforming to maximize IRS potential for wireless

communication enhancement [20], [21], [22], [23]. In a double-IRS system, the IRSs are placed near the base station and near the devices, enhancing their communication performance. This system introduces new degrees of freedom through a double-reflection link across the two IRSs, providing additional benefits when direct and single-reflection links are blocked [20], [21]. Zheng et al. showed the effectiveness of cooperative passive beamforming (CPB) when multiple IRSs are deployed to enhance wireless communication performance because the traditional approach of decoupled passive beamforming design becomes suboptimal [23]. This is because the inter-IRS channels play a significant role in the system's overall performance and must be considered. In this scenario, passive beamforming across multiple IRSs should be cooperatively designed to take advantage of the multiplicative beamforming gain and to avoid undesired interference. By jointly optimizing passive beamforming across multiple IRSs, interference can be minimized, and the system can benefit from the additional gain achieved through their collective operation. Studies have shown that if the double-reflection channel is line-of-sight (LoS), it can achieve a higher passive beamforming-gain scaling order than each single-reflection link as the number of reflecting elements (L) becomes large: ($O(L^4)$) versus $O(L^2)$) [24]. This gain is attributed to the CPB advantage over the inter-IRS LoS channel. This promising performance of the double-IRS system led to investigations using more than two IRSs in a wireless network to further enhance communications performance. By appropriately assigning multiple IRSs to help different links simultaneously, overall system performance can be further improved.

Despite the aforementioned advantages of deploying single and multiple IRSs to improve network performance, passive IRS-aided systems face a specific limitation known as *double-fading attenuation*. This is due to the fact that reflected signals must pass through a cascaded channel consisting of transmitter-IRS and IRS-receiver links. This limitation significantly constrains signal power at the receiver and limits the effective coverage of each IRS [25]. The proposed solutions to address the practical issues of the passive IRS include two approaches: deploying more passive elements, and adjusting IRS proximity. However, equipping the IRS with a large number of reflecting elements can be technically challenging and costly. It requires careful design, fabrication, and installation, which may not be feasible or cost-effective in real-world scenarios. The other approach involves placing a passive IRS closer to either the transmitter or the receiver. By reducing the distance between the IRS and the transceivers, the cascaded channel path loss can be mitigated, leading to improved signal power and coverage. However, this proximity adjustment can also present practical limitations [26]. In light of these practical challenges and complexities, researchers have been exploring alternative solutions such as active IRS technology. Active IRS enables simultaneous signal reflection and amplification, offering a more efficient way to compensate for the cascaded path loss without the need for an excessive number of reflecting elements. An active IRS shows promise in overcoming the limitations faced by the passive IRS, and holds the potential to significantly improve wireless communications performance in a more practical and effective manner [27], [28], [29], [30], [31], [32], [33], [34], [35], [36]. The key technology in an active intelligent reflecting surface is the simultaneous signal reflection and amplification capability. Unlike the conventional passive IRS, where the reflecting elements do not actively amplify signals, the active IRS introduces active elements with a signal amplification capability. Zhang et al. showed that in a typical wireless system, active IRSs can achieve a significant sum-rate gain of 130% [27], superior to the passive IRS at only 22%, thus overcoming the double-fading attenuation effect. Zeng et al. considered a single active IRS deployment in a WPCN and exploited the potential benefits of an active IRS by maximizing the weighted sum throughput to guarantee throughput fairness [29]. In [37], [38] and [39] the authors presented hybrid approaches for active and passive elements on the same surface, and compared the superior performance of a hybrid active/passive IRS with single or multiple passive IRSs in wireless networks. Dong et al. showed that a hybrid architecture has a 40% improvement over the conventional IRS-aided system [37]. Fu and Zhang considered distributed pairing of an active IRS and a passive IRS, and discussed the deployment of IRS elements in the uplink throughput maximization problem [40]. However, there is still a need to study hybrid active/passive IRSs to design the resources in WPCNs.

There are some existing studies exploiting the benefits of integration of WPCNs with single/multiple active and passive IRSs [2], [5], [8], [13], [18], [19], [29], [35], [41], [42], [43], [44], [45] and references therein. [29], [35], [44] considered a single active IRS deployment in a WPCN and exploited the potential benefits of an active IRS by maximizing the throughput of the network. However, in most existing work on IRS-assisted WPCNs, researchers mainly focus on comparison of an active IRS to single/multiple passive IRSs. In [45], Fu et al. presented the study on the downlink WIT/WPT from a multi-antenna base station to a single-antenna user over a multi-active/passive IRS (AIRS/PIRS)-enabled wireless link. The optimal active IRS deployment for multi-AIRS/PIRS enabled WIT and WPT is presented. To the best of our knowledge there is no prior work is done on the hybrid active and passive assisted WPCNs. When we introduce a pair of active and passive IRSs, multiple reflection links can boost the wireless link capacity and improve network performance. Hence, To exploit the benefits of multiple reflection, we propose a novel architecture for the WPCN with the pairing of an active IRS and a passive IRS. Nevertheless, it becomes more challenging to design joint deployment of active and passive IRS elements due to the joint operations of downlink WET and uplink WIT in WPCNs. In particular, by employing active IRS elements capable of signal amplification, new

optimization variables and constraints arise, making the joint design of resource allocation and joint active/passive IRS beamforming on downlink and uplink highly challenging. Amplified thermal noise in the active IRS also becomes a crucial consideration, impacting both downlink wireless energy transfer and uplink wireless information transfer. On uplink, achieving a balance between maximizing received signal power and minimizing noise adds to the complexity. Addressing the complexities effectively demands innovative and non-trivial efforts to harness the full potential of hybrid active/passive IRS technology for improved WPCN performance. To the best of our knowledge this is the first work that studies hybrid distributed active and passive IRSs in WPCNs. The main contributions of this paper are as follows.

- We propose a novel, hybrid active and passive IRS-aided architecture for a WPCN, which combines the benefits of active- and double-IRS effects to enhance overall network performance. The system consists of both active and passive IRS elements working together to assist WET on downlink and WIT on uplink. In this architecture, we jointly optimize active and passive beamforming strategies on both downlink and uplink to achieve throughput fairness in the WPCN. To address the challenge of the doubly-near-far problem, where devices may experience significantly different received signal strengths, we maximize the minimum throughput of all end-user devices. This optimization involves jointly optimizing the amplitude and phase shift matrices of active and passive IRS elements, along with the time allocations for WET and WIT. Leveraging the advantages of the active IRS, we optimize the amplitude of the incident signals to further improve overall network performance.
- The throughput fairness problem formulated in the hybrid active/passive IRS-aided architecture is non-convex and highly complex, making it numerically challenging to solve directly. To address this, a divide-and-conquer approach is adopted, breaking down the main problem into three sub-problems as follows, and iteratively solving them until convergence is achieved. *Active and Passive Downlink Beamforming Optimization:* In this step, the time allocations and uplink optimization variables are fixed, converting the problem into a semi-definite program (SDP). The approach uses semidefinite relaxation (SDR) and the penalty function method to find a near-optimal solution for active and passive beamforming. *Active and Passive Uplink Beamforming Optimization:* With time allocations and downlink optimization variables fixed, this sub-problem is addressed using a provably convergent successive convex approximation (SCA)-based second-order cone programming (SOCP) approach. The active and passive beamformers are updated simultaneously in each iteration to find a solution. *Downlink and Uplink Time Allocations Optimization:*In the final step, active and passive beamforming are fixed, and the problem is converted into convex form. The Lagrangian optimization method is applied to find the optimal solution for time allocations. By dividing the main problem into these three sub-problems and iteratively solving them, the divide-and-conquer approach overcomes the numerical complexity and non-convexity of the throughput fairness problem in the hybrid active/passive IRS-aided architecture. This approach helps achieve near-optimal solutions for joint optimization of active and passive beamforming and time allocations, ensuring improved network performance and throughput fairness.
- We explore two practical scenarios for deployment of the active/passive IRS in a network. In *Hybrid Case-1*, we deploy the active IRS near the hybrid access point and the passive IRS near the devices. In *Hybrid Case-2*, we deploy the active IRS near the devices and the passive IRS near the H-AP. Through extensive simulations and numerical analysis, we demonstrate that *Hybrid Case-1* outperforms *Hybrid Case-2*. We also compare the performance of the proposed active/passive IRS-aided WPCN with a system that uses an active single-IRS and another system with a conventional passive double-IRS. The results show that the proposed hybrid system performs significantly better in terms of network performance and throughput fairness, making it a superior choice for practical deployment in WPCNs.

The rest of the paper is organized as follows. In Section II, we define the system model of the hybrid active/passive-IRS WPCN, and we formulate the throughput fairness problem. The solution proposed for the formulated problem is explained in Section III. We analyze complexity notations and convergence of the proposed algorithm in Section IV. We discuss the set parameters for numerical analysis, and present simulation results, in Section V. Finally, we discuss the conclusions of our findings in Section VI. Important notations and their definitions are in Table 1.

II. SYSTEM MODEL AND PROBLEM FORMULATION

In this paper, we consider the hybrid, active/passive IRS-aided wireless powered communication network shown in Fig. 1, which consists of a single-antenna hybrid access point, IRS-1 equipped with L_1 reflecting elements, IRS-2 equipped with L_2 reflecting elements, and K wireless devices denoted, $\{u_1, u_2, \ldots, u_K\}$, with a single antenna each. The IRSs are attached to a smart controller to dynamically tune the reflecting coefficients of the IRSs (also called *reflect beamforming*) to reconfigure the incident wave with the desired phase and amplitude adjustments. Moreover, an active load is attached to the active IRS, which enables the IRS to amplify the coefficients of incident signals to the level needed to meet network QoS. IRS-1 is placed near the H-AP, and IRS-2 is placed near the devices. The communication channels from H-AP to IRS-1, from H-AP to IRS-2, from IRS-1 to IRS-2, from IRS-1 to the k_{th} user, and from IRS-2 to the k_{th} user are showing as $\mathbf{g}_1 \in \mathbb{C}^{L_1 \times 1}$,

TABLE 1. Notations.

Symbol	Definitions
$x \in A$	x is the element in set A
$\|a\|$	The absolute value of a complex-valued scalar a
$\|\|\mathbf{a}\|\|$	The norm of a complex-valued vector a
$[\mathbf{A}]_{a,b}$	The element in matrix $\mathbf{A}$ positioned at a_{th} row and b_{th} column
$\text{diag}(\mathbf{a})$	The diagonal matrix of vector $\mathbf{a}$
$\text{Tr}(\mathbf{A})$	The trace of matrix $\mathbf{A}$
$\text{rank}(\mathbf{A})$	The rank of matrix $\mathbf{A}$
$(\mathbf{a})^H$	The conjugate transpose of a complex-valued vector $\mathbf{a}$
$\mathbf{A} \succcurlyeq 0$	Positive semidefinite matrix $\mathbf{A}$
j	The imaginary unit, i.e., $j^2 = -1$
$\mathbb{C}^{a\times b}$	The space of $a \times b$ complex-valued matrices

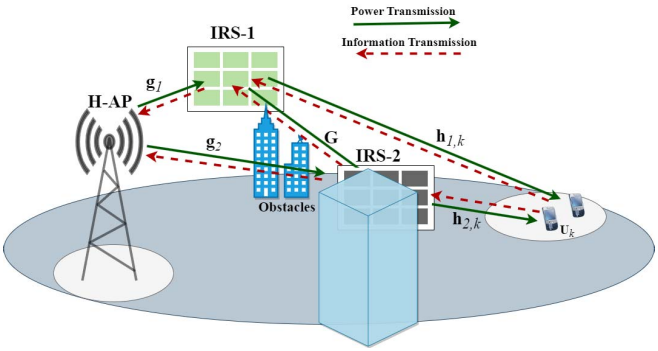

FIGURE 1. A hybrid active/passive IRS-assisted WPCN that consists of a single-antenna H-AP, distributed active and passive IRSs with L_1, and L_2 reflecting elements, respectively, and K wireless devices. There is no direct link between the H-AP and wireless devices because of obstacles. The H-AP transmits wireless energy on downlink and the devices transmit wireless information on uplink.

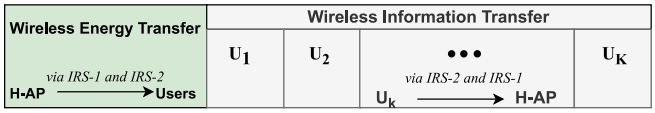

FIGURE 2. A TDD frame-based scheme: the coherence time interval is split in two. In the first part, the H-AP broadcasts an energy signal to all devices via IRS-1 and IRS-2. The second part is divided into K slots in which the devices transmit information signals to the H-AP.

$\mathbf{g}_2 \in \mathbb{C}^{L_2\times 1}$,$\mathbf{G} \in \mathbb{C}^{L_1\times L_2}$, $\mathbf{h}_{1,k} \in \mathbb{C}^{L_1\times 1}$ and $\mathbf{h}_{2,k} \in \mathbb{C}^{L_1\times 1}$, respectively. The direct channel between the H-AP and the devices is blocked by obstacles, so the IRSs are deployed to assist with wireless energy transfer and wireless information transfer. However, the proposed algorithm is extendable to a case with direct links between the H-AP and the devices. The downlink (DL) channels transmit wireless energy from the H-AP to the devices, and the uplink (UL) channels transfer information signals from devices to the H-AP. UL and DL channels are assumed to be quasi-static, flat fading channels that remain constant during the whole coherence interval, denoted T, but they can vary from one coherence interval to another. However, instantaneous channel state information is assumed to be stored in the transmitter at the beginning of the coherence interval.

Nevertheless the perfect channel estimation is challenging but there are some preliminary studies have been done on channel estimation of IRS-assisted networks. Reference [46] presented a novel three-phase framework for precise channel estimation in IRS-enabled uplink multiuser communication systems. This framework harnesses IRS channel correlations, employing LMMSE estimators to address challenges in reducing estimation time, error propagation, and optimizing pilot power allocation. In [47], author proposed an efficient always-ON reflection channel estimation protocol for uplink cascaded channels in IRS-aided MU-MISO setups with the significant reduction in pilot overhead. Reference [48] presented an efficient uplink channel estimation scheme for the double-IRS aided multi-user MIMO system with both IRSs always turned ON during the entire channel training for maximizing their reflected signal power which are shown to achieve high channel estimation accuracy with practically low training overhead. Without loss of generality, we set $T = 1$ for the rest of the paper.

The total coherence interval is divided into two phases, as shown in Fig. 2. In the first phase, the H-AP transmits wireless energy on downlink in time slot t_0, and devices harvest energy and store it in embedded rechargeable batteries. It is assumed that devices have no active power source and use the harvested energy for communications on uplink. The second phase is further divided into K time slots denoted $\{t_1, t_2, , t_K\}$, in which u_k sends an information signal in the k_{th} time slot.

A. DOWNLINK POWER TRANSMISSION

During downlink power transmission, the H-AP broadcasts energy signal x_e, $E[|x_e|^2] = 1$, to the devices via IRS-1 and IRS-2. From here, we consider IRS-1 the active IRS where an active load is attached to the IRS to amplify the incident signal, and IRS-2 is considered the passive IRS, which can only adjust the phase of the incident signal without amplification. The transmitted signal reaches the devices via both active and passive IRSs (IRS-1 and IRS-2). Thus, the signal received at the k_{th} user is

$$y_k = \sqrt{P_t}\left(h_{2,k}^H \Gamma_{2,d} \mathbf{G}^H \Gamma_{1,d} \mathbf{g}_1 + \mathbf{h}_{2,k}^H \Gamma_{2,d} \mathbf{g}_2 + \mathbf{h}_{1,k}^H \Gamma_{1,d} \mathbf{g}_1\right) x_0 + \left(h_{2,k}^H \Gamma_{2,d} G^H \Gamma_{1,d} + h_{1,k}^H \Gamma_{1,d}\right) z_{IRS} + z_k, \quad \forall k, \qquad (1)$$

Here, P_t is the transmission power at the H-AP; $\Gamma_{i,d} = \text{diag}\{\alpha_{i,1}e^{j\theta_{i,1}}, \alpha_{i,2}e^{j\theta_{i,2}}, \ldots, \alpha_{i,L_i}e^{j\theta_{i,L_i}}\}$ for $i \in [1,2]$ shows the downlink reflection matrices for IRS-1 and IRS-2; $\alpha_{1,l} \in [0, \alpha_{l,max}]$, $\alpha_{l,max} \geq 1$, is the reflection coefficient of the l_{th} reflection element in the active IRS, and $\alpha_{2,l} \in [0,1]$ is the reflection coefficient of l_{th} reflection element in passive IRS. However, $\theta_{i,l} \in [0, 2\pi]$, $i = 1,2$ is the reflection phase of the l_{th} element in IRS-1 and IRS-2; $\mathbf{z}_{IRS} \in \mathbb{C}^{L_1 \times 1}$ and z_k represent the thermal noise at IRS-1 and the k_{th} user, respectively, distributed as $\mathcal{CN}(\mathbf{0}, \sigma_I^2\mathbf{I}_{L_1})$ and $\mathcal{CN}(0, \sigma_k^2)$, respectively. Unlike the passive IRS, thermal noise at the active IRS cannot be ignored because the active IRS has the ability to amplify the incident signal. However, we can ignore energy harvesting by z_k.

Proposition 1: We define $\mathbf{Q}_k = \text{diag}(\mathbf{g}_I)\mathbf{G}\text{diag}(\mathbf{h}_{2,k}) \in \mathbb{C}^{L_1 \times L_2}$, $\mathbf{Q}_{2,k} = \mathbf{G}\text{diag}(\mathbf{h}_{2,k}) \in \mathbb{C}^{L_1 \times L_2}$, $\mathbf{g}_{1,k} = \text{diag}(\mathbf{g}_I)\mathbf{h}_{1,k} \in \mathbb{C}^{L_1 \times 1}$, and $\mathbf{g}_{2,k} = \text{diag}(\mathbf{g}_2)\mathbf{h}_{2,k} \in \mathbb{C}^{L_2 \times 1}$ as cascaded links between H-AP $\rightarrow$ IRS-1 $\rightarrow$ IRS-2 $\rightarrow$ k_{th} user, IRS-1 $\rightarrow$ IRS-2 $\rightarrow$ k_{th} user, H-AP $\rightarrow$ IRS-1 $\rightarrow$ k_{th} user, and H-AP $\rightarrow$ IRS-2 $\rightarrow$ k_{th} user, respectively. By defining $\mathbf{v}_d = [\alpha_{1,1}e^{j\theta_{1,1}}, \alpha_{1,2}e^{j\theta_{1,2}}, \ldots, \alpha_{1,L_1}e^{j\theta_{1,L_1}}]^H$ and $\mathbf{w}_d = [\alpha_{2,1}e^{j\theta_{2,1}}, \alpha_{2,2}e^{j\theta_{2,2}}, \ldots, \alpha_{2,L_2}e^{j\theta_{2,L_2}}]^H$ we can rewrite Eq. (1) as

$$y_k = \sqrt{P_t}\Big(w_d^H Q_k^H v_d + g_{1,k}^H v_d + g_{2,k}^H w_d\Big)x_0 + \Big(\Gamma_{2,d}\mathbf{Q}_{2,k}^H\Gamma_{1,d} + h_{1,k}^H\Gamma_{1,d}\Big)z_{IRS} + z_k, \quad \forall k, \quad (2)$$

The total energy harvested at u_k, as transmitted by the H-AP via IRS-1 and IRS-2 is expressed as

$$E_k = \varsigma_k t_0 P_t\left|\mathbf{w}_d^H\mathbf{Q}_k^H\mathbf{v}_d + \mathbf{g}_{1,k}^H\mathbf{v}_d + \mathbf{g}_{2,k}^H\mathbf{w}_d\right|^2 + \varsigma_k t_0\sigma_I^2\left(\left|\mathbf{w}_d^H\mathbf{Q}_{2,k}^H\mathbf{v}_d\right|^2 + \left|\mathbf{h}_{1,k}^H\mathbf{v}_d\right|^2\right), \quad \forall k, \quad (3)$$

where $0 < \varsigma_k < 1$ is energy harvesting efficiency at the k_{th} receiver.

B. UPLINK INFORMATION TRANSMISSION

After the devices harvest energy during the downlink phase, in the next uplink information transmission phase, they send independent information signals to the H-AP in their allocated time slots. We assume all the energy harvested by each user is utilized to send information on uplink. In time slot t_k, u_k sends information signal $x_k \sim \mathcal{CN}(0, p_k)$ to the H-AP, in which p_k denotes the average transmit power available at u_k, which is given by

$$p_k(t_0, t_k, \mathbf{v}_d, \mathbf{w}_d) = \frac{E_k(t_0, \mathbf{v}_d, \mathbf{w}_d)}{t_k} \quad (4)$$

The signal received at the H-AP as sent by u_k via IRS-2 and IRS-1 is given by

$$r_k = \sqrt{p_k}\Big(g_I^H\Gamma_{1,u}G\Gamma_{2,u}h_{2,k} + g_2^H\Gamma_{2,u}h_{2,k} + g_I^H\Gamma_{1,u}h_{1,k}\Big)x_k + g_I^H\Gamma_{1,u}z_{IRS} + z_A, \quad \forall k, \quad (5)$$

where $z_A \sim \mathcal{CN}(0, \sigma_A^2)$ is noise at the H-AP, and $\Gamma_{i,u} = \text{diag}\{\beta_{i,1}e^{j\omega_{i,1}}, \beta_{i,2}e^{j\omega_{i,2}}, \ldots, \beta_{i,L_i}e^{j\omega_{i,L_i}}\}$ for $i \in [1,2]$ is the uplink reflection matrices for IRS-1 and IRS-2, in which $\beta_{1,l} \in [0, \beta_{l,max}]$, $\beta_{l,max} \geq 1$, is the reflection coefficient of the l_{th} reflection element in the active IRS, and $\beta_{2,l} \in [0,1]$ is the reflection coefficient of the l_{th} reflection element in the passive IRS. However, $\omega_{i,l} \in [0, 2\pi]$, $i = 1,2$, is the reflection phase of the l_{th} element in IRS-1 and IRS-2.

Proposition 2: We define $\mathbf{v}_u = [\beta_{1,1}e^{j\omega_{1,1}}, \beta_{1,2}e^{j\omega_{1,2}}, \ldots, \beta_{1,L_1}e^{j\omega_{1,L_1}}]^H$ and $\mathbf{w}_u = [\beta_{2,1}e^{j\omega_{2,1}}, \beta_{2,2}e^{j\omega_{2,2}}, \ldots, \beta_{2,L_2}e^{j\omega_{2,L_2}}]^H$ and using *Proposition 1*, we can rewrite Eq. (5) as

$$r_k = \sqrt{p_k}\Big(\mathbf{v}_u^H Q_k\mathbf{w}_u + \mathbf{g}_{1,k}^H\mathbf{v}_u + \mathbf{g}_{2,k}^H\mathbf{w}_u\Big)x_k + g_I^H\Gamma_{1,u}z_{IRS} + z_A, \quad \forall k, \quad (6)$$

The achievable uplink throughput of u_k in bits per second per hertz (bps/Hz) is

$$R_k(p_k, t_k, \mathbf{v}_u, \mathbf{w}_u) = t_k\log_2\left[1 + \frac{p_k\left|\mathbf{v}_u^H Q_k\mathbf{w}_u + \mathbf{g}_{1,k}^H\mathbf{v}_u + \mathbf{g}_{2,k}^H\mathbf{w}_u\right|^2}{\sigma_I^2\left|g_I^H\mathbf{v}_u\right|^2 + \sigma_A^2}\right], \quad \forall k, \quad (7)$$

C. THROUGHPUT-FAIRNESS OPTIMIZATION PROBLEM

In this section, we discuss the challenges of the doubly-near-far problem in wireless networks, particularly when employing multiple IRS elements. From Eq. (3) and Eq. (7), we observe that a nearby user with better channel conditions can harvest more energy and achieves higher throughput than the distant user, which creates an imbalance in the system. This issue is exacerbated by cascaded channel path loss. Additionally, harvested energy and throughput depend on both uplink and downlink time allocations, but due to the total time constraint, increasing both simultaneously is not feasible. To address this problem, we propose throughput fairness optimization to maximize the minimum throughput among devices by jointly optimizing active and passive beamforming and time allocations on both uplink and downlink. Therefore, from Eqs. (3) to (7), we can formulate the throughput fairness problem as follows:

$$\mathcal{P}1 \max_{t_0, \{t_k\}, \mathbf{v}_d, \mathbf{w}_d, \mathbf{v}_u, \mathbf{w}_u} \min_k R_k(p_k, t_k, v_u, w_u) \quad (8a)$$

$$\text{s.t. } P_t\left|g_I^H\mathbf{v}_d\right|^2 + \sigma_I^2\|\mathbf{v}_d\|^2 \leq P_{RIS} \quad (8b)$$

$$p_k\left|h_{I,k}^H\mathbf{v}_u\right|^2 + \sigma_I^2\|\mathbf{v}_u\|^2 \leq P_{RIS}, \quad \forall k \quad (8c)$$

$$|[\mathbf{v}_d]_l| \leq \alpha_{l,max}, \quad l = 1,2,3,\ldots L_1 \quad (8d)$$

$$|[\mathbf{w}_d]_l| = 1, \quad l = 1,2,3,\ldots L_2 \quad (8e)$$

$$|[\mathbf{v}_u]_l| \leq \beta_{l,max}, \quad l = 1,2,3,\ldots L_1, \quad (8f)$$

$$|[\mathbf{w}_u]_l| = 1, \quad l = 1,2,3,\ldots L_2 \quad (8g)$$

$$\sum_{j=0}^{K} t_j \leq 1; \quad t_j \geq 0 \quad (8h)$$

In $\mathcal{P}1$, (8a) shows the maximization of minimum throughput among all K devices. Unlike a passive IRS, an

active IRS introduces new constraints: (8b), (8c), and (8d). Constraints (8b) and (8c) are amplification power constraints in which P_{RIS} is the available amplification power budget in the active IRS, and (8d) is the limitation on power amplification. An active IRS is allowed to allocate available power to extend the amplitude of incident signals with active loads after consuming power with the hardware. However, incident signal amplification is limited to a predetermined maximum amplitude: $\alpha_{l,max}$, $\beta_{l,max}$ for downlink and uplink, respectively. However, a passive IRS only adjusts the phase of passive elements, and cannot amplify the incident signal. Therefore, in constraint (8e) for a passive IRS, the amplitude of the incident signal is limited to 1, and (8f) is the total time constraint on downlink and uplink.

Owing to the non-convex objective function and highly coupled optimal variable constraints, $\mathcal{P}1$ is highly complex, and difficult to solve analytically. Therefore, we divide the problem into sub-problems and solve them using SDP and SCA techniques.

III. PROPOSED ALGORITHM FOR $\mathcal{P}1$

From $\mathcal{P}1$, we see that the formulated problem is highly complex and difficult to solve due to highly coupled variables and non-convexity of objective functions and constraints. Therefore, to solve $\mathcal{P}1$, we decompose the problem into three sub-problems and solve them in turn. In the first stage, we exploit semidefinite relaxation to solve for downlink beamforming and find a near-optimal solution for active and passive phase shift matrices and amplitude coefficients of the active IRS. In the next stage, we find a near optimal solution for uplink beamforming by both active and passive IRSs by using SCA technique. In the last stage, we use the Lagrangian method to optimize time allocations for downlink and uplink transmissions.

A. ACTIVE AND PASSIVE DOWNLINK BEAMFORMING OPTIMIZATION

In this stage, we first optimize the active and passive downlink beamforming vectors for phase and amplitude coefficients by fixing the uplink beamforming matrices and time allocations. For fixed uplink active and passive beamforming, $\mathbf{w}_u$, $\mathbf{v}_u$, and time allocation $\{t_0, t_1, \ldots, t_k\}$, problem $\mathcal{P}1$ is reduced to the following harvesting power maximization problem to design the downlink passive and active beamforming vectors (constant/irrelevant terms are omitted for brevity).

$$\mathcal{P}1.A \quad \max_{\mathbf{v}_d, \mathbf{w}_d} \ \min_k p_k(\mathbf{v}_d, \mathbf{w}_d) \tag{9a}$$

$$\text{s.t.} \ \ (8b), \ (8c), \ (8d), \ (8e) \tag{9b}$$

Here, we introduce a slack variable γ, and the equivalent problem can be written as

$$\mathcal{P}1.A \quad \max_{\gamma, \mathbf{v}_d, \mathbf{w}_d} \ \gamma \tag{10a}$$

$$\text{s.t.} \ \ \varsigma_k \frac{t_0}{t_k} P_t \left| \mathbf{w}_d^H \mathbf{Q}_k^H \mathbf{v}_d + \mathbf{g}_{1,k}^H \mathbf{v}_d + \mathbf{g}_{2,k}^H \mathbf{w}_d \right|^2 + \varsigma_k \frac{t_0}{t_k} \sigma_I^2 \left(\left| \mathbf{w}_d^H \mathbf{Q}_{2,k}^H \mathbf{v}_d \right|^2 + \left| \mathbf{h}_{1,k}^H \mathbf{v}_d \right|^2 \right) \geq \gamma \quad \forall k \tag{10b}$$

$$(9b) \tag{10c}$$

Nonetheless, it is still challenging to solve $\mathcal{P}1.A$ due to the coupling of $\mathbf{v}_d$ and $\mathbf{w}_d$ in constraint (10b). Moreover, $\mathcal{P}1.A$ is still non-convex and difficult to solve optimally due to unit-modulus constraint (8e). Therefore, we propose to alternatively optimize the active and passive beamforming vectors by fixing one and then the other. Hereafter, we use the SDR technique to transform $\mathcal{P}1.A$ into a convex problem. In particular, for the given $\mathbf{w}_d$, we solve $\mathcal{P}1.A$ for $\mathbf{v}_d$, and the equivalent problem can be written as

$$\mathcal{P}1.A.1 \quad \max_{\gamma, \mathbf{v}_d} \ \gamma \tag{11a}$$

$$\text{s.t.} \ \ (8b), \ (8c), \ (8d), (10b) \tag{11b}$$

Proposition 3: We define $\mathbf{f}_k^H = \mathbf{w}_d^H \mathbf{Q}_k^H + \mathbf{g}_{1,k}^H$, and $q_k = \mathbf{g}_{2,k}^H \mathbf{w}_d$. We can represent $|\mathbf{w}_d^H \mathbf{Q}_k^H \mathbf{v}_d + \mathbf{g}_{1,k}^H \mathbf{v}_d + \mathbf{g}_{2,k}^H \mathbf{w}_d|^2 = |\mathbf{f}_k^H \mathbf{v}_d + q_k|^2 = \bar{\mathbf{v}}_d^H \mathbf{F_k} \bar{\mathbf{v}}_d + |q_k|^2$, given that $\mathbf{F_k} = [\mathbf{f}_k \mathbf{f}_k^H, \ \mathbf{f}_k q_k; \ q_k^H \mathbf{f}_k^H, \ \mathbf{0}] \in \mathbb{C}^{(L_1+1)\times(L_1+1)}$ and $\bar{\mathbf{v}}_d = [\mathbf{v}_d \ \ 1]^H \in \mathbb{C}^{(L_1+1)\times 1}$. Furthermore, we define $\mathbf{G}_1 = \mathbf{g}_1 \mathbf{g}_1^H$, $\mathbf{H}_{1,k} = \mathbf{h}_{1,k} \mathbf{h}_{1,k}^H$, $\tilde{\mathbf{Q}}_{2,k} = \mathbf{Q}_{2,k} \mathbf{w}_d \mathbf{w}_d^H \mathbf{Q}_{2,k}^H$ and $\mathbf{V}_d = \bar{\mathbf{v}}_d \bar{\mathbf{v}}_d^H$ which requires $\mathbf{V}_d \succcurlyeq 0$ and $\text{rank}(\mathbf{V}_d) = 1$.

By dropping the rank-1 constraint, we can transform $\mathcal{P}1.A$ into relaxed convex problem as follows:

$$\mathcal{P}1.A.1 \quad \max_{\gamma, \mathbf{V}_d} \ \gamma \tag{12a}$$

$$\text{s.t.} \ \ 0 \geq \frac{\gamma}{A_k} - B\text{Tr}\left(\bar{\mathbf{Q}}_{2,k} \mathbf{V}_d\right) - B\text{Tr}\left(\bar{\mathbf{H}}_{1,k} \mathbf{V}_d\right) - \text{Tr}(\mathbf{V}_d \mathbf{F_k}) - |q_k|^2, \quad \forall k \tag{12b}$$

$$0 \geq A_k \left(\text{Tr}(\mathbf{V}_d \mathbf{F_k}) + |q_k|^2 \right) + B\text{Tr}\left(\bar{\mathbf{Q}}_{2,k} \mathbf{V}_d\right) + B\text{Tr}\left(\bar{\mathbf{H}}_{1,k} \mathbf{V}_d\right) - C_k, \quad \forall k \tag{12c}$$

$$0 \geq \text{Tr}\left(\bar{\mathbf{G}}_1 \mathbf{V}_d\right) + B\text{Tr}(\mathbf{V}_d) - P_{RIS} \tag{12d}$$

$$\mathbf{V}_d \succcurlyeq 0 \tag{12e}$$

where $\bar{\mathbf{H}}_{1,k}$, $\bar{\mathbf{Q}}_{2,k}$, and $\bar{\mathbf{G}}_1$ are matrices with extra zero rows and columns, and $A_k = \varsigma_k \frac{t_0}{t_k} P_t$, $B = \frac{\sigma_I^2}{P_t}$, and $C_k = \frac{P_{IRS} - \sigma_I^2 \|\mathbf{v}_u\|^2}{\|\mathbf{h}_{1,k}^H \mathbf{v}_u\|^2}$. $\mathcal{P}1.A.1$ is an SDP and can be efficiently solved with existing convex optimization solvers such as MATLAB CVX [49]. However, the SDR technique might not lead to a rank-one solution, but we can retrieve a feasible rank-one solution to $\mathcal{P}1.A.1$ by converting the rank-one constraint into a tractable convex constraint.

rank-1 Constraint: By using an exact penalty function method, we can write the equivalent form of the rank-one constraint as $\text{Tr}(\mathbf{V}_d) \leq \lambda_1(\mathbf{V}_d)$ given that λ_1 is the largest eigenvalue of $\mathbf{V}_d$ and where strict equality holds if $\text{rank}\mathbf{V}_d = 1$. We thus have the following optimization problem

$$\mathcal{P}1.A.1 \quad \max_{\gamma, \mathbf{V}_d} \ \gamma - \delta(\text{Tr}(\mathbf{V}_d) - \lambda_1(\mathbf{V}_d)) \tag{13a}$$

$$\text{s.t.} \ \ (12b), \ (12c), \ (12d), \ (12e) \tag{13b}$$

where δ is the penalty factor. We can efficiently solve $\mathcal{P}1.A.1$ by adjusting the value of the penalty factor that gives the rank-one solution. However, Problem (12) is still non-convex because of the $\lambda_1(\mathbf{V}_d)$ term in the objective function. To handle this, we exploit the SCA technique by approximating this term by its first-order Taylor series approximation, which is a global lower bound because $\lambda_1(\mathbf{V}_d)$ is convex. Hence, we derive the Taylor underestimation of $\lambda_1(\mathbf{V}_d)$ as

$$\lambda_1(\mathbf{V}_d) \geq \lambda_1\left(\mathbf{V}_d^{(n)}\right) + \mathbf{x_1}^{(n)H}\left(\mathbf{V}_d - \mathbf{V}_d^{(n)}\right)\mathbf{x_1}^{(n)} \tag{14}$$

where $\mathbf{x_1}^{(n)}$ is the corresponding eigenvector of λ_1 in the n_{th} iteration.

By incorporating Eq. (14) into Problem (13), the solving method of $\mathcal{P}1.A.1$ becomes iterative and can be more time-consuming if its variables are not initialized properly. Therefore, for fast convergence in the solution, an initial feasible point was generated by exploiting a feasible point pursuit method [50]. For this, the slack variables $\mathbf{s}_1 = [s_{1,1}, s_{1,2}, \ldots s_{1,K}]$, $\mathbf{s}_2 = [s_{2,1}, s_{2,2}, \ldots s_{2,K}]$ and s_3 are introduced to generate a feasible point in the following problem:

$$\min_{\substack{\gamma,\mathbf{V}_d,\\ \mathbf{s}_1,\mathbf{s}_2,s_3}} \quad \sum_{k=1}^{K} s_{1,k} + \sum_{k=1}^{K} s_{2,k} + s_3 \tag{15a}$$

$$\text{subject to} \quad 0 \geq \frac{\gamma}{A_k} - B\mathrm{Tr}\left(\bar{\mathbf{Q}}_{2,k}\mathbf{V}_d\right) - B\mathrm{Tr}\left(\bar{\mathbf{H}}_{1,k}\mathbf{V}_d\right) - \mathrm{Tr}(\mathbf{V}_d\mathbf{F_k}) - |q_k|^2 - s_{1,k}, \quad \forall k \tag{15b}$$

$$0 \geq A_k\left(\mathrm{Tr}(\mathbf{V}_d\mathbf{F_k}) + |q_k|^2\right) + B\mathrm{Tr}\left(\bar{\mathbf{Q}}_{2,k}\mathbf{V}_d\right) + B\mathrm{Tr}\left(\bar{\mathbf{H}}_{1,k}\mathbf{V}_d\right) - C_k - s_{2,k}, \quad \forall k \tag{15c}$$

$$0 \geq \mathrm{Tr}\left(\bar{\mathbf{G}}_1\mathbf{V}_d\right) + B\mathrm{Tr}(\mathbf{V}_d) - P_{RIS} - s_3 \tag{15d}$$

$$\mathbf{V}_d \succcurlyeq 0; s_i \geq 0; \quad i = 1, 2, 3 \tag{15e}$$

By solving Problem (15), we extract the initial values of eigenvalue $\lambda_1(\mathbf{V}_d^{(0)})$ and corresponding eigenvector $\mathbf{x_1}^{(0)}$ by using eigenvalue decomposition (EVD). Then, we solve Problem (13) in iterations until convergence is achieved. In each iteration, the optimal solution of Problem (13) $[\mathbf{V}_d^{(n)}, \mathbf{s}_1^{(n)}, \mathbf{s}_2^{(n)}, s_3^{(n)}]$ is achieved, which is a feasible point in n_{th} iteration.

Next, we optimize the passive beamforming vector $\mathbf{w}_d$ for the given $\mathbf{v}_d$, where $\mathcal{P}1.A$ is equivalent to

$$\mathcal{P}1.A.2 \quad \max_{\gamma,\mathbf{w}_d} \quad \gamma \tag{16a}$$

$$\text{s.t.} \quad (8c), \ (8e), \ (10b) \tag{16b}$$

Following the similar transformation for $\mathcal{P}1.A.1$ in (11)-(14), we can solve $\mathcal{P}1.A.2$ using SDR and SCA as well. Hence, by defining, $\mathbf{s}_k = \mathbf{Q}_k^H\mathbf{v}_d + \mathbf{g}_{2,k}$, and $m_k = \mathbf{g}_{1,k}^H\mathbf{v}_d$. Equivalently, $|\mathbf{w}_d^H\mathbf{Q}_k^H\mathbf{v}_d + \mathbf{g}_{1,k}^H\mathbf{v}_d + \mathbf{g}_{2,k}^H\mathbf{w}_d|^2 = |\mathbf{w}_d^H\mathbf{s}_k + m_k|^2 = \bar{\mathbf{w}}_d^H\mathbf{S}\bar{\mathbf{w}}_d + |m_k|^2$, given that $\mathbf{S_k} = [\mathbf{s}_k\mathbf{s}_k^H, \ \mathbf{s}_k m_k^H; \ m_k\mathbf{s}_k^H, \ \mathbf{0}] \in \mathbb{C}^{(L_2+1)\times(L_2+1)}$ and $\bar{\mathbf{w}}_d = [\mathbf{w}_d \ \ 1]^H \in \mathbb{C}^{(L_2+1)\times 1}$. Further, by defining $\tilde{\mathbf{S}}_{2,k} = \mathbf{Q}_{2,k}^H\mathbf{v}_d\mathbf{v}_d^H\mathbf{Q}_{2,k}$, and $\mathbf{W}_d = \bar{\mathbf{w}}_d\bar{\mathbf{w}}_d^H$ which requires $\mathbf{W}_d \succcurlyeq 0$ and $\mathrm{rank}(\mathbf{W}_d) = 1$.

$\mathcal{P}1.A.2$ can be equivalently be written as

$$\mathcal{P}1.A.2 \quad \max_{\gamma,\mathbf{W}_d} \quad \gamma - \delta\left[\mathrm{Tr}(\mathbf{W}_d) - (\rho_1(\mathbf{W}_d^{(n)}) + \boldsymbol{\phi_1}^{(n)H}(\mathbf{W}_d - \mathbf{W}_d^{(n)})\boldsymbol{\phi_1}^{(n)})\right] \tag{17a}$$

$$\text{s.t.} \quad 0 \geq \frac{\gamma}{A_k} - B\mathrm{Tr}\left(\mathbf{W}_d\bar{\mathbf{S}}_{2,k}\right) - D_k - \mathrm{Tr}(\mathbf{W}_d\mathbf{S_k}) - |m_k|^2, \quad \forall k \tag{17b}$$

$$0 \geq A_k\left(\mathrm{Tr}(\mathbf{W}_d\mathbf{S_k}) + |m_k|^2\right) + D_k + B\mathrm{Tr}\left(\mathbf{W}_d\bar{\mathbf{S}}_{2,k}\right) - C_k, \quad \forall k \tag{17c}$$

$$\mathbf{W}_d \succcurlyeq 0 \tag{17d}$$

where $\boldsymbol{\phi_1}^{(n)}$ is the corresponding eigenvector of the largest eigenvalue ρ_1 of $\mathbf{W}_d$ in the n_{th} iteration and $D_k = B\|\mathbf{h}_{1,k}^H\mathbf{v}_d\|^2$.

B. ACTIVE AND PASSIVE UPLINK BEAMFORMING OPTIMIZATION

In this sub-problem, we optimize the active and passive beamforming vectors for uplink by fixing the other optimal variables, specifically, the given downlink beamforming vector, $\mathbf{v}_d$, $\mathbf{w}_d$, and the time allocations $\{t_0, t_1, \ldots, t_k\}$. To tackle the max-min problem in $\mathcal{P}1$, we introduce an auxiliary variable and rewrite the problem for designing the uplink beamforming vectors, $\mathbf{v}_u$, $\mathbf{w}_u$.

$$\mathcal{P}1.B \ \max_{\eta,\mathbf{v}_u,\mathbf{w}_u} \quad \eta \tag{18a}$$

$$\text{s.t.} \quad t_k \log_2\left[1 + \frac{p_k\left|\mathbf{v}_u^H Q_k\mathbf{w}_u + \mathbf{g}_{1,k}^H\mathbf{v}_u + \mathbf{g}_{2,k}^H\mathbf{w}_u\right|^2}{\sigma_I^2\left|g_I^H\mathbf{v}_u\right|^2 + \sigma_A^2}\right] \geq \eta \tag{18b}$$

$$(8c), \ (8f), \ (8g) \tag{18c}$$

The problem is still challenging to solve owing to non-convex constraint (18b). The following lemmas can be used to transform $\mathcal{P}1.B$ into a solvable formulation.

Lemma 1 [51]: For any x and y, we have the following inequality

$$\ln\left(1 + \frac{|x|^2}{y}\right) \geq \ln\left(1 + \frac{|\bar{x}|^2}{\bar{y}}\right) - \frac{|\bar{x}|^2}{\bar{y}} + \frac{2\mathcal{R}\{\bar{x}^H x\}}{\bar{y}} - \left[\frac{|\bar{x}|^2}{\bar{y}}\right]\left[\frac{y + |\bar{x}|^2}{\bar{y} + |\bar{x}|^2}\right] \tag{19}$$

Based on Lemma 1, a lower bound is imposed on constraint (18b) to find a solvable convex form of $\mathcal{P}1.B$.

Proposition 4: For a fixed $\mathbf{w}_u$, we define $\mathbf{X}_k = \mathbf{Q}_k\mathbf{w}_u + \mathbf{g}_{1,k}$, and $Y_k = \mathbf{g}_{2,k}^H\mathbf{w}_u$. We can reformulate $\mathcal{P}1.B$ as follows:

$$\mathcal{P}1.B.1 \ \max_{\eta,\mathbf{v}_u} \quad \eta \tag{20a}$$

$$\text{s.t.} \quad \ln\left(1 + \frac{p_k\left|\mathbf{v}_u^{(n)H}\mathbf{X}_k + Y_k\right|^2}{\sigma_I^2\left|\mathbf{g}_1^H\mathbf{v}_u^{(n)}\right|^2 + \sigma_A^2}\right)$$

$$
\begin{aligned}
&- \frac{p_k\left|\mathbf{v}_u^{(n)^H}\mathbf{X}_k + Y_k\right|^2}{\sigma_I^2\left|\mathbf{g}_1^H\mathbf{v}_u^{(n)}\right|^2 + \sigma_A^2} \\
&+ \frac{2\mathcal{R}\left\{p_k\left(\mathbf{v}_u^{(n)^H}\mathbf{X}_k + Y_k\right)^H\left(\mathbf{v}_u^H\mathbf{X}_k + Y_k\right)\right\}}{\sigma_I^2\left|\mathbf{g}_1^H\mathbf{v}_u^{(n)}\right|^2 + \sigma_A^2} \\
&- \left[\frac{p_k\left|\mathbf{v}_u^{(n)^H}\mathbf{X}_k + Y_k\right|^2}{\sigma_I^2\left|\mathbf{g}_1^H\mathbf{v}_u^{(n)}\right|^2 + \sigma_A^2}\right] \\
&\times\left[\frac{\sigma_I^2\left|\mathbf{g}_1^H\mathbf{v}_u\right|^2 + \sigma_A^2 + p_k\left|\mathbf{v}_u^H\mathbf{X}_k + Y_k\right|^2}{\sigma_I^2\left|\mathbf{g}_1^H\mathbf{v}_u^{(n)}\right|^2 + \sigma_A^2 + p_k\left|\mathbf{v}_u^{(n)^H}\mathbf{X}_k + Y_k\right|^2}\right] \geq \frac{\eta}{t_k} \qquad (20b)
\end{aligned}
$$

$$
(8c),\ (8f) \qquad (20c)
$$

where $\mathbf{v}_u^{(n)}$ shows the solution to $\mathcal{P}1.B.1$ in the n_{th} iteration. Hence, we iteratively solve convex problem $\mathcal{P}1.B.1$ using the CVX solver until convergence is achieved.

Similarly, for a fixed $\mathbf{v}_u$, we define $\mathbf{J}_k = \mathbf{v}_u^H\mathbf{Q}_k + \mathbf{g}_{2,k}$, and $Z_k = \mathbf{g}_{I,k}^H\mathbf{v}_u$. Using Lemma 1, we can reformulate $\mathcal{P}1.B$ as follows:

$$
\begin{aligned}
\mathcal{P}1.B.2 \quad &\max_{\eta,\mathbf{w}_u} \ \eta \qquad (21a) \\
&\text{s.t. } \ln\left(1 + E_k\left|\mathbf{J}_k\mathbf{w}_u^{(n)} + Z_k\right|^2\right) \\
&\quad - E_k\left|\mathbf{J}_k\mathbf{w}_u^{(n)} + Z_k\right|^2 \\
&\quad + 2\mathcal{R}\left\{E_k\left(\mathbf{J}_k\mathbf{w}_u^{(n)} + Z_k\right)^H\left(\mathbf{J}_k\mathbf{w}_u^{(n)} + Z_k\right)\right\} \\
&\quad - \left(E_k\left|\mathbf{J}_k\mathbf{w}_u^{(n)} + Z_k\right|^2\right) \times \\
&\quad \left[\frac{1 + E_k|\mathbf{J}_k\mathbf{w}_u + Z_k|^2}{1 + E_k\left|\mathbf{J}_k\mathbf{w}_u^{(n)} + Z_k\right|^2}\right] \geq \frac{\eta}{t_k} \qquad (21b) \\
&\quad |[\mathbf{w}_u]_l| \ = 1, \quad l = 1, 2, 3, \ldots L_2 \qquad (21c)
\end{aligned}
$$

where $E_k = \frac{p_k}{\sigma_I^2|\mathbf{g}_1^H\mathbf{v}_u|^2 + \sigma_A^2}$ and $\mathbf{w}_u^{(n)}$ shows the solution to $\mathcal{P}1.B.2$ in the n_{th} iteration. However, we are left with the non-convexity of constraint (21c) because of the unit-modulus term. So, we tackle this equality by first relaxing it to an inequality constraint, i.e. $|[\mathbf{w}_u]_l| \ \leq 1, \quad l = 1, 2, 3, \ldots L_2$ and then we redefine the objective function as $\eta - \zeta\|\mathbf{w}_u\|^2$, where ζ is the regularization term. If it is sufficiently large, the optimal solution of $\mathcal{P}1.B.2$ can be obtained when convergence is achieved. Note the concavity term, $-\zeta\|\mathbf{w}_u\|^2$, in the objective function. However, we can convexify the objective function using first-order Taylor approximation. In summary, the equivalent convex $\mathcal{P}1.B.2$ to solve uplink passive beamforming vector $\mathbf{w}_u$ is given by

$$
\begin{aligned}
\mathcal{P}1.B.2 \quad &\max_{\eta,\mathbf{w}_u} \ \eta - \zeta\left\{2\mathcal{R}\left(\mathbf{w}_u^{(n)^H}\mathbf{w}_u\right) - \|\mathbf{w}_u^{(n)}\|^2\right\} \qquad (22a) \\
&\text{s.t. } |[\mathbf{w}_u]_l| \ \leq 1, \quad l = 1, 2, 3, \cdots L_2 \qquad (22b) \\
&\quad (21b) \qquad (22c)
\end{aligned}
$$

C. DOWNLINK AND UPLINK TIME ALLOCATIONS OPTIMIZATION

In this subsection, we tackle downlink and uplink time optimization in $\mathcal{P}1$ by fixing the uplink and downlink beamforming vectors. To be specific, the time allocation problem for given $\{\mathbf{w}_d, \mathbf{v}_d, \mathbf{w}_u, \mathbf{v}_u\}$ is

$$
\begin{aligned}
\mathcal{P}1.C \quad &\max_{\eta,t_0,\{t_k\}} \ \eta \qquad (23a) \\
&\text{s.t. } \ t_k\log_2\left[1 + M_k\frac{t_0}{t_k}\right] \geq \eta \qquad (23b) \\
&\quad (8c),\ (8h) \qquad (23c)
\end{aligned}
$$

where $M_k = \frac{\varsigma_k(P_t|\mathbf{w}_d^H\mathbf{Q}_k^H\mathbf{v}_d + \mathbf{g}_{I,k}^H\mathbf{v}_d + \mathbf{g}_{2,k}^H\mathbf{w}_d|^2 + \sigma_I^2|\mathbf{h}_{I,k}^H\mathbf{v}_d|^2)}{\sigma_I^2|g_I^H\mathbf{v}_u|^2 + \sigma_A^2} \times \frac{|\mathbf{v}_u^HQ_k\mathbf{w}_u + \mathbf{g}_{I,k}^H\mathbf{v}_u + \mathbf{g}_{2,k}^H\mathbf{w}_u|^2m}{\sigma_I^2|g_I^H\mathbf{v}_u|^2 + \sigma_A^2}$. The optimal value of η^* will be the maximum value of all feasible solutions under constraint (23b). To solve $\mathcal{P}1.C$, we first consider the feasibility problem of throughput-fairness optimization. Hence, for any $\eta > 0$, the time allocation optimization problem is written as

$$
\begin{aligned}
\mathcal{P}1.C \quad &\text{Find } \ [t_0, t_1, \ldots t_K] \qquad (24a) \\
&\text{s.t. } \ (23b),\ (8c),\ (8h) \qquad (24b)
\end{aligned}
$$

Since $\mathcal{P}1.C$ is a standard convex optimization problem, we can solve it using the Lagrangian dual optimization method [6], [52]. The Lagrangian function of $\mathcal{P}1.C$ is given by

$$
\begin{aligned}
\mathcal{L}(\eta, t_0, t_k, \mu, \chi_k, \vartheta_k) = \eta &+ \sum_{k=1}^{K}\chi_k\left(t_k\log_2\left[1 + M_k\frac{t_0}{t_k}\right] - \eta\right) \\
&+ \mu\left(1 - \sum_{j=0}^{K}t_j\right) \\
&+ \sum_{k=1}^{K}\vartheta_k(t_kN_k - t_0) \qquad (25)
\end{aligned}
$$

where N_k is the constant term in (8c), and μ, $\boldsymbol{\chi} = [\chi_1, \chi_2, \ldots \chi_K]^T$, $\boldsymbol{\vartheta} = [\vartheta_1, \vartheta_2, \ldots \vartheta_K]^T$ are the non-negative Lagrangian multiplier. Therefore, the dual function is

$$
\mathcal{D}(\mu, \boldsymbol{\chi}, \boldsymbol{\vartheta}) = \max_{\eta,t_0,t_k} \mathcal{L}(\eta, t_0, t_k, \mu, \boldsymbol{\chi}, \boldsymbol{\vartheta}) \qquad (26)
$$

The dual problem is

$$
\begin{aligned}
\mathcal{P}1.C \text{ (dual)} \quad &\min_{\mu,\boldsymbol{\chi},\boldsymbol{\vartheta}} \ \mathcal{D}(\mu, \boldsymbol{\chi}, \boldsymbol{\vartheta}) \qquad (27a) \\
&\text{s.t. } \ \mu \geq 0, \boldsymbol{\chi} \succcurlyeq 0, \boldsymbol{\vartheta} \succcurlyeq 0 \qquad (27b)
\end{aligned}
$$

Lemma 2: For the given $(\eta, \mu, \boldsymbol{\chi}, \boldsymbol{\vartheta})$, optimal time allocation solution $\{t_0^*, \{t_k\}^*\}$ is given by

$$
t_0^* = \frac{1}{1 + \sum_{k=1}^{K}\Lambda_k^*} \qquad (28)
$$

$$
t_k^* = \frac{\Lambda_k^*}{1 + \sum_{k=1}^{K}\Lambda_k^*}, \quad \forall k \qquad (29)
$$

Algorithm 1 The Proposed SDR and Penalty Function Method-Based Algorithm to Solve $\mathcal{P}1.A$

Set the initial values for $\mathbf{w}_u$, $\mathbf{v}_u$, time allocation $\{t_0, t_1, \ldots, t_k\}$, tolerance value ξ
// *main loop*:
repeat
  Set the initial values for $\mathbf{w}_d$
  Find the initial feasible solution for given $\gamma^{(0)}$, and obtain $\lambda_1(\mathbf{V}_d^{(0)})$ and $\mathbf{x_1}^{(0)}$ using CVX solver and compute $f_o^{(0)} = \gamma^{(0)} - \delta(Tr(\mathbf{V}_d^{(0)}) - \lambda_1(\mathbf{V}_d^{(0)})$
  // *initial loop*:
  $i = 0$
  repeat
    Solve Problem (13) using MATLAB CVX solver and compute $\mathbf{V}_d^{(i)*}, \gamma^{(i)*}, f_o^{(i)*}$
    $i = i + 1$
    Assign $f_o^{(i)} \leftarrow f_o^{(i-1)*}$, $\mathbf{V}_d{}^{(i)} \leftarrow \mathbf{V}_d^{(i-1)*}$, $\gamma^{(i)} \leftarrow \gamma^{(i-1)*}$,
  until $\frac{\left|f_o^{(i)} - f_o^{(i-1)}\right|}{f_o^{(i-1)}} \leq \xi$
  // *main loop*:
  Assign $\mathbf{V}_d^* \leftarrow \mathbf{V}_d^{(i)}$
  Compute $\bar{\mathbf{v}}_d^* \approx \sqrt{\lambda_1}\mathbf{x}_1$
  Extract $\mathbf{v}_d^*$ by definition described in *Proposition 3*
  Next
  Set the value for $\mathbf{v}_d = \mathbf{v}_d^*$
  Do steps 5-17 to find $\mathbf{w}_d^*$ by solving Problem (17)
  Assign $\mathbf{w}_d^* \leftarrow \mathbf{w}_d^{(i)}$
until convergence achieved
output $\mathbf{v}_d^*, \mathbf{w}_d^*$

where Λ_k^* can be found by solving the Karush-Kuhn-Tucker (KKT) conditions of the Lagrangian function in (25).

Proof: See Appendix A.

With feasible optimal solution $\{t_0^*, \{t_k\}^*\}$, we update $(\mu, \boldsymbol{\chi}, \boldsymbol{\vartheta})$ by using the following sub-gradient method:

$$\chi_k^{i+1} = \left[\chi_k^i - \Delta_1^i\left(t_k^* \log_2\left[1 + M_k \frac{t_0^*}{t_k^*}\right] - \eta\right)\right]^+, \quad \forall k \tag{30}$$

$$\vartheta_k^{i+1} = \left[\vartheta_k^i - \Delta_2^i(t_k N_k - t_0)\right]^+, \quad \forall k \tag{31}$$

$$\mu^{i+1} = \left[\mu^i - \Delta_3^i\left(1 - \sum_{j=0}^{K} t_j\right)\right]^+ \tag{32}$$

where $[x]^+ = max(0, x)$, i is the iteration number and $\{\Delta_1, \Delta_2, \Delta_3\}$ are the step sizes for the updates. We iteratively solve for $(\mu^*, \boldsymbol{\chi}^*, \boldsymbol{\vartheta}^*)$ when convergence is achieved. However, we will find η^* by using a bisection search. We summarize the time allocation procedure in Algorithm 3.

IV. CONVERGENCE AND COMPLEXITY ANALYSIS

The complete algorithm of our proposed solution is presented in Algorithm 4 and graphical explanation is presented in Fig. 3.

Algorithm 2 The Proposed SCA Based Algorithm to Solve $\mathcal{P}1.B$

Set the initial values for $\mathbf{w}_d$, $\mathbf{v}_d$, time allocation $\{t_0, t_1, \ldots, t_k\}$, tolerance value ξ
// *main loop*:
repeat
  Set the initial values for $\mathbf{w}_u$
  // *initial loop*:
  $n = 1$
  repeat
    Solve Problem $\mathcal{P}1.B$ using MATLAB CVX solver and compute $\mathbf{v}_u^{(n)*}, \eta^{(n)*}$
    $n = n + 1$
    Assign $\eta^{(n)} \leftarrow \eta^{(n-1)*}$, $\mathbf{v}_u{}^{(n)} \leftarrow \mathbf{v}_u^{(n-1)*}$
  until $\frac{\eta^{(n)} - \eta^{(n-1)}}{\eta^{(n-1)}} \leq \xi$
  // *main loop*:
  Assign $\mathbf{v}_u^* \leftarrow \mathbf{v}_u^{(n)}$
  Next
  Set the value for $\mathbf{v}_u = \mathbf{v}_u^*$
  Find the initial feasible solution for given $\eta^{(0)}$ and $\mathbf{w}_u^{(0)}$
  // *initial loop*:
  $n = 1$
  repeat
    Solve Problem (22) using MATLAB CVX solver and compute $\mathbf{w}_u^{(n)*}, \eta^{(n)*}, f_o^{(n)*} = \eta - \zeta\left\{2\mathcal{R}\left(\mathbf{w}_u^{(n-1)^H}\mathbf{w}_u^{(n)^*}\right) - \|\mathbf{w}_u^{(n-1)}\|^2\right\}$
    $n = n + 1$
    Assign $f_o^{(n)} \leftarrow f_o^{(n-1)*}$, $\mathbf{w}_u{}^{(n)} \leftarrow \mathbf{w}_u^{(n-1)*}$, $\eta^{(n)} \leftarrow \eta^{(n-1)*}$,
  until $\frac{\left|f_o^{(n)} - f_o^{(n-1)}\right|}{f_o^{(n-1)}} \leq \xi$
  // *outer loop*:
  Assign $\mathbf{w}_u^* \leftarrow \mathbf{w}_u^{(n)}$
  Next
  Set the value for $\mathbf{w}_u = \mathbf{w}_d^*$
until convergence achieved
output $\mathbf{w}_u^*, \mathbf{v}_u^*$

A. CONVERGENCE PROPERTY

In the subsequent analysis, we examine the convergence of the proposed solution based on Algorithm 1- Algorithm 3. Assuming the optimal solution of (13) is denoted as $\mathbf{V}_d^{(n)}$, we can verify the iterative Problem (13) for convergence as follows:

$$\begin{aligned} f\left(\mathbf{V}_d^{(n+1)}\right) &= \gamma - \delta\left(\mathrm{Tr}\left(\mathbf{V}_d^{(n+1)}\right) - \lambda_1\left(\mathbf{V}_d^{(n+1)}\right)\right) \\ &\geq \gamma - \delta\left(\mathrm{Tr}\left(\mathbf{V}_d^{(n+1)}\right) - \lambda_1\left(\mathbf{V}_d^{(n)}\right)\right. \\ &\quad \left. - \mathbf{x_1}^{(n)H}\left(\mathbf{V}_d^{(n+1)} - \mathbf{V}_d^{(n)}\right)\mathbf{x_1}^{(n)}\right) \\ &\geq \gamma - \delta\left(\mathrm{Tr}\left(\mathbf{V}_d^{(n)}\right) - \lambda_1\left(\mathbf{V}_d^{(n)}\right)\right. \\ &= f\left(\mathbf{V}_d^{(n)}\right) \end{aligned} \tag{33}$$

Similarly, we can prove that the optimal solution of (18) is $\mathbf{W}_d^{(n)}$. It can be verified that the objective function of Problem (9) is non-decreasing and convergent if

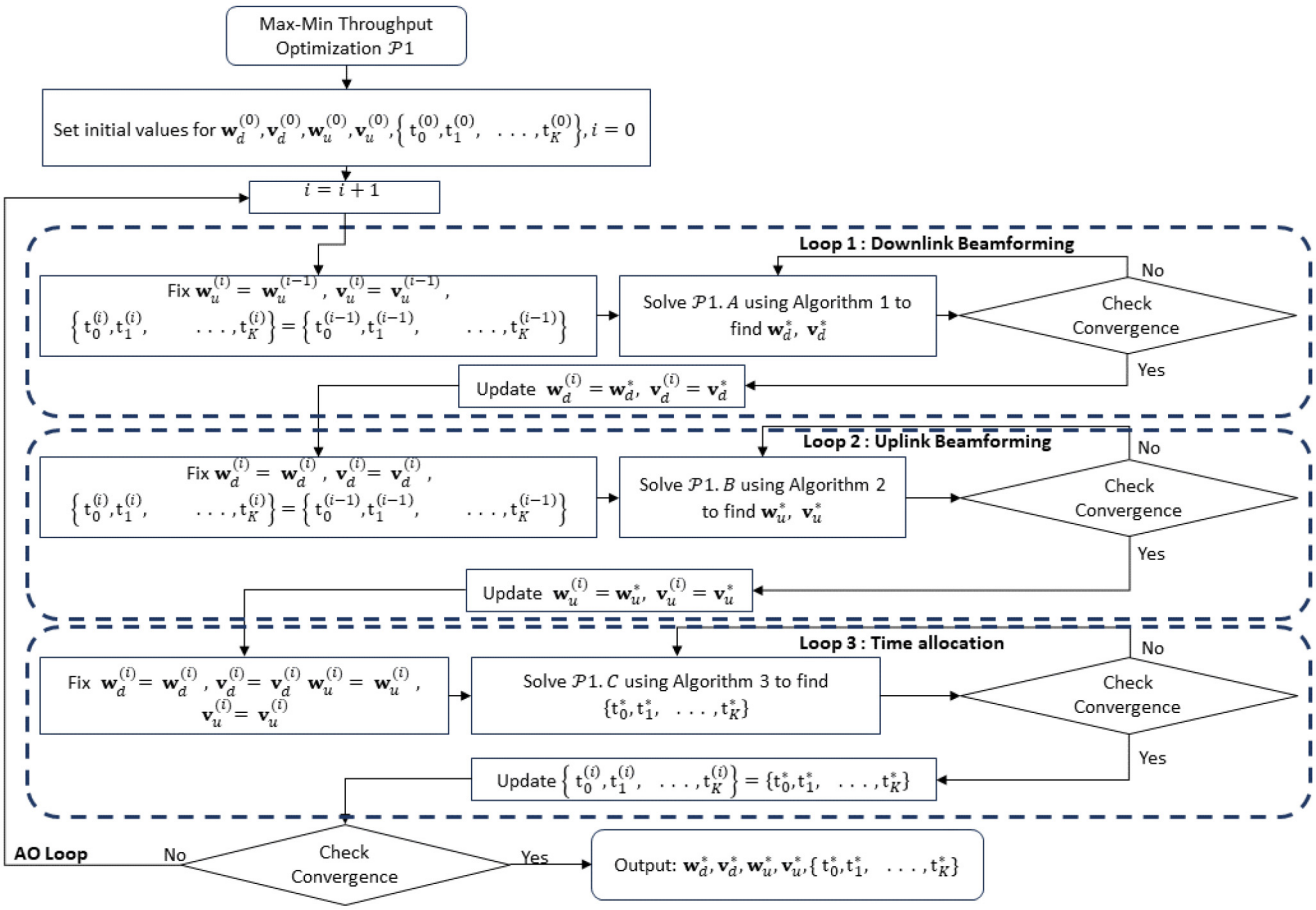

FIGURE 3. The flowchart of the proposed solution.

Algorithm 3 The Proposed Lagrangian Optimization Method and Bisection Search-Based Algorithm to Solve Problem $\mathcal{P}1.C$

Set the initial values for $\mathbf{w}_d$, $\mathbf{v}_d$, $\mathbf{w}_u$, $\mathbf{v}_u$, η_{min}, η_{max}, μ, $\boldsymbol{\chi}$, $\boldsymbol{\vartheta}$, ϵ
repeat
  $\eta \leftarrow \frac{\eta_{min}+\eta_{max}}{2}$
  Solve $\mathcal{P}1.C$ using *Lemma 2* and find optimal solution for $\{t_0^*, \{t_k\}^*\}$
  Compute $\mathcal{D}(\mu, \boldsymbol{\chi}, \boldsymbol{\vartheta})$ using (25) and check for the feasibility of the solution
  if $\mathcal{D}(\mu, \boldsymbol{\chi}, \boldsymbol{\vartheta}) > \eta$, solution is infeasible, set $\eta_{max} \leftarrow \eta$ and go to step 4
  else Update $\mu, \boldsymbol{\chi}, \boldsymbol{\vartheta}$ using (30)-(32), and go to step 5 until stopping criterion of sub-gradient method achieved
  set $\eta_{min} \leftarrow \eta$
until $\eta_{max} - \eta_{min} \leq \epsilon$
output $\eta^*, t_0^*, \{t_k\}^*$

Algorithm 4 The Proposed SDR, SCA and Lagrangian Optimization-Based Algorithm to Solve Problem $\mathcal{P}1$

Set the initial values for $\mathbf{w}_d$, $\mathbf{v}_d$, $\mathbf{w}_u$, $\mathbf{v}_u$, η, μ, $\boldsymbol{\chi}$, $\boldsymbol{\vartheta}$, ϵ, $\{t_0, t_1, \ldots, t_k\}$, ξ
Set $i = 0$, and compute $min\{R_k^{(0)}\}$ using Eq. (7) with initialized variables
repeat
  Solve $\mathcal{P}1.A$ to obtain $\{\mathbf{w}_d^{(i)}, \mathbf{v}_d^{(i)}\}$ with fixed $\{\mathbf{w}_u^{(i-1)}, \mathbf{v}_u^{(i-1)}, \{t_0, t_1, \ldots, t_k\}^{(i-1)}\}$ using Algorithm 1
  Solve $\mathcal{P}1.B$ to obtain $\{\mathbf{w}_u^{(i)}, \mathbf{v}_u^{(i)}\}$ with fixed $\{\mathbf{w}_d^{(i)}, \mathbf{v}_d^{(i)}, \{t_0, t_1, \ldots, t_k\}^{(i-1)}\}$ using Algorithm 2
  Solve $\mathcal{P}1.C$ to obtain $\{t_0, t_1, \ldots, t_k\}^{(i)}$ with fixed $\{\mathbf{w}_d^{(i)}, \mathbf{v}_d^{(i)}, \mathbf{w}_u^{(i)}, \mathbf{v}_u^{(i)}\}$ using Algorithm 3
  Compute $min\{R_k^{(i)}\}$ using Eq. (7) and check for the feasibility of the solution
  if $min\{R_k^{(i)}\} < min\{R_k^{(i-1)}\}$, solution is infeasible, go to step 4
  else $i = i + 1$, and go to step 4
until $min\{R_k^{(i)}\} - min\{R_k^{(i-1)}\} \leq \epsilon$
output $\mathbf{w}_d^*, \mathbf{v}_d^*, \mathbf{w}_u^*, \mathbf{v}_u^*, t_0^*, \{t_k\}^*$

Constraints (10b) and (10c) are satisfied, given that $\mathbf{V}_d$ and $\mathbf{W}_d$ are bounded by (8d) and (8e), respectively.

The feasibility condition of the optimal solution in the n^{th} iteration must adhere to Constraints (10b) and (10c). Algorithm 2 also produces a non-decreasing objective function, i.e., $f(\mathbf{v}_u^{(n+1)}, \mathbf{w}_u^{(n+1)}) \geq f(\mathbf{v}_u^{(n)}, \mathbf{w}_u^{(n)})$, where $f(\mathbf{v}_u^{(n)}, \mathbf{w}_u^{(n)})$ is the feasible solution in the n^{th} iteration.

Furthermore, due to the inequality in (19) and the satisfaction of Constraints (8f) and (8g), the objective function remains bounded, ensuring convergence.

With the optimal solution of $\mathbf{v}_d^{(i)}, \mathbf{w}_d^{(i)}, \mathbf{v}_u^{(i)}, \mathbf{w}_u^{(i)}, t_0^{(i)}, t_k^{(i)}$ in the i^{th} iteration in Algorithm 4, the objective function of Problem (8) is: $f_{\mathcal{P}1}(\mathbf{v}_u^{(i+1)}, \mathbf{w}_u^{(i+1)}, \mathbf{v}_d^{(i+1)}, \mathbf{w}_d^{(i+1)}, t_0^{(i+1)}, \{t_k^{(i+1)}\}) \geq f_{\mathcal{P}1}(\mathbf{v}_u^{(i+1)}, \mathbf{w}_u^{(i+1)}, \mathbf{v}_d^{(i+1)}, \mathbf{w}_d^{(i+1)}, t_0^{(i)}, \{t_k^{(i)}\}) \geq f_{\mathcal{P}1}(\mathbf{v}_u^{(i)}, \mathbf{w}_u^{(i)}, \mathbf{v}_d^{(i+1)}, \mathbf{w}_d^{(i+1)}, t_0^{(i)}, \{t_k^{(i)}\}) \geq f_{\mathcal{P}1}(\mathbf{v}_u^{(i)}, \mathbf{w}_u^{(i)}, \mathbf{v}_d^{(i)}, \mathbf{w}_d^{(i)}, t_0^{(i)}, \{t_k^{(i)}\})$. This sequence of inequalities demonstrates that the algorithm's objective function is guaranteed to converge.

B. COMPLEXITY ANALYSIS

Here, we analyze the computational complexity of Algorithm 4, which is a combination of the complexities of three sub-problems in Steps 4-7.

In Step 4, we solve the SDR problem for active and passive downlink beamforming vectors, which involves $L_1 + L_2 + 2$ variables and $4K + 3$ constraints. The computational complexity for this step is $\mathcal{O}1(I_1(I1a[(L_1+1)^{0.5}((L_1+1)^6+(L_1+1)^2(2K+2))] + I_{1b}[(L_2+1)^{0.5}((L_2+1)^6+(L_2+1)^2(2K+1))]))$, where I_1, I_{1a}, and I_{1b} represent the iteration numbers of the outer and inner iterations in Algorithm 1. Similarly, in Step 5, we solve the SCA problem for active and passive uplink beamforming vectors, which involves L_1+L_2+2 and $4K+L_1+L_2+2$ variables, respectively. The computational complexity for this step is $\mathcal{O}2(I_2(I2a[(2K+2L_1+2)^{3.5}] + I_{2b}[(2K+2L_2+2)^{3.5}]))$, where I_2, I_{2a}, and I_{2b} represent the iteration numbers of the outer and inner iterations in Algorithm 2. In Step 6, we solve the time allocations using the Lagrangian dual method and Bisection search, which has a computational complexity of $\mathcal{O}3(I_3 I_{3a}(K+1)^2)$, where I_3 and I_{3a} stand for the BS and inner iterations, respectively, in Algorithm 3. Finally, the total computational complexity of Algorithm 4 is $\mathcal{O}4(I_T[\mathcal{O}1+\mathcal{O}2+\mathcal{O}3])$, where I_T represents the total number of iterations in Algorithm 4.

V. NUMERICAL RESULTS AND DISCUSSIONS

In this section, we provide and discuss numerical results to validate the proposed schemes and to evaluate the performance of the hybrid active and passive IRS in WPCNs. Under the simulation setup, we consider a three-dimensional Cartesian coordinate system. The H-AP, IRS-1, and IRS-2 are located at $(0, 0, 0)$, $(1, 1, 5)$, and $(3, -1, 5)$, respectively (in meters). However, devices are randomly and uniformly distributed centered at $(3, 0, 0)$ within a radius of 0.5m. The distance dependent path loss is modeled as $P_L = L_0 \frac{D^{-\Omega}}{D_0}$, where L_0 is signal attenuation at a reference distance of 1m and set at $-30dB$ and Ω is the path loss exponent set at 2.2 for all links. Moreover, direct links between H-AP and users are blocked by obstacles so the IRSs assist wireless communication between H-AP and devices. However, reflected links are modeled with Rician fading given by

$$\mathbf{g} = \sqrt{\frac{\kappa}{1+\kappa}}\mathbf{g}^{LOS} + \sqrt{\frac{1}{1+\kappa}}\mathbf{g}^{NLOS}, \tag{34}$$

where κ is the Rician factor set to 3, $\mathbf{g}^{NLOS}$ denotes the non-line-of-sight (NLOS) standard Rayleigh fading components with zero mean and unit variance, and $\mathbf{g}^{LOS}$ is a line-of-sight (LOS) component that can be modeled using a far-field uniform linear array (ULA) [53], given as $\mathbf{g}^{LOS} = [1\ e^{-j2\pi\frac{s}{\lambda}\sin(\theta)} \ldots\ e^{-j2\pi\frac{s}{\lambda}(L-1)\sin(\theta)}]^T$ in which s shows the spacing between IRS elements (which is considered $\lambda/2$), and θ is the angle-of-departure (AOD) or angle-of-arrival (AOA) of the IRS elements. The other parameters are set for total transmit power budget at H-AP and active IRS as $P_T = 30$dBm, $P_{IRS} = 30$dBm, respectively,[1] the noise power at H-AP and IRS as $\sigma_A^2 = \sigma_I^2 = -70$dBm, and the energy harvesting efficiency $\varsigma_k = \varsigma = 0.8$, for all k.

In order to show the effectiveness of hybrid active and passive IRSs in a WPCN, we consider the following basic schemes in the simulations for comparison and analysis.

1) *Single Active IRS:* In a single active IRS, we deploy an IRS with L elements, which is placed near the H-AP. Here, we jointly optimize uplink and downlink beamforming amplification coefficients and phase shifts with time allocations.
2) *Hybrid Active/Passive IRSs (proposed):* From Fu and Zhang, we noticed it is important to find the optimal position or placement of the active IRS between the H-AP and the devices [40]. Thus, in hybrid active/passive IRSs, we discuss two different cases in which we deploy the active IRS in different places as shown in Fig. 4. In the first case, denoted *Hybrid Case-1*, we deploy the active IRS near the H-AP and the passive IRS near the devices, which is formulated and solved in Eqs. (1)-(30). However, in *Hybrid Case-2*, we deploy the active IRS near the devices and the passive IRS near the H-AP. We explain the problem formulation and the proposed solution for *Hybrid Case-2* in Appendix B.
3) *Double Passive IRSs:* Here, we consider two passive IRSs and jointly optimize the phase shift matrices and time allocations for uplink and downlink. For this we fix the amplification coefficients of IRSs $\alpha_{1,l} = \alpha_{2,l} = \beta_{1,l} = \beta_{2,l} = 1$, for $l \in [1, 2, 3, \ldots L_1$ or $L_2]$ in Eqs. (1)-(30).

We provide a convergence analysis of the proposed algorithms. Fig. 5 illustrates the convergence of Algorithm 1 and Algorithm 2 based on the SDR and SCA methods, respectively. The graphs demonstrate that both methods exhibit rapid convergence, reaching a solution at or before the fifth iteration across different values of L. Additionally, we display the convergence of the alternating optimization-based Algorithm 4 in Fig. 6, which jointly solves the throughput fairness problem by combining all the sub-problems. The results show that the algorithm yields feasible solutions where the minimum throughput increases in each iteration, indicating successful convergence. These convergence analyses validate the effectiveness and efficiency of

1. For fairer performance comparison we set transmission power equal in all schemes. For double passive IRSs scheme, we set the transmission power to 33.1 dBm.

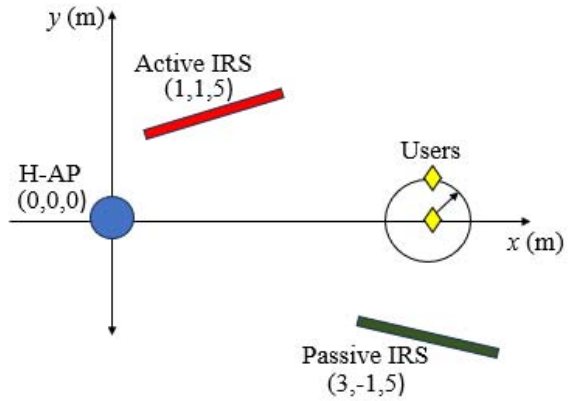

(a) Hybrid Case-1

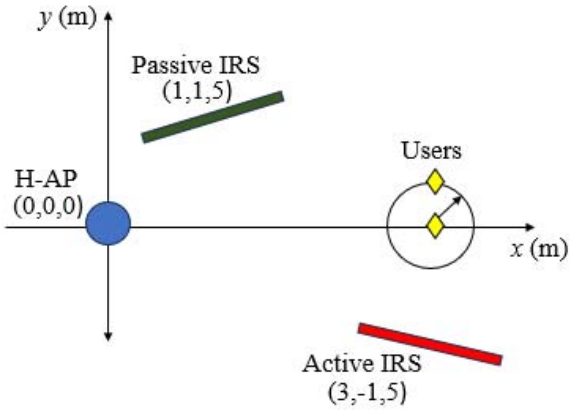

(b) Hybrid Case-2

FIGURE 4. Top view of simulation setup.

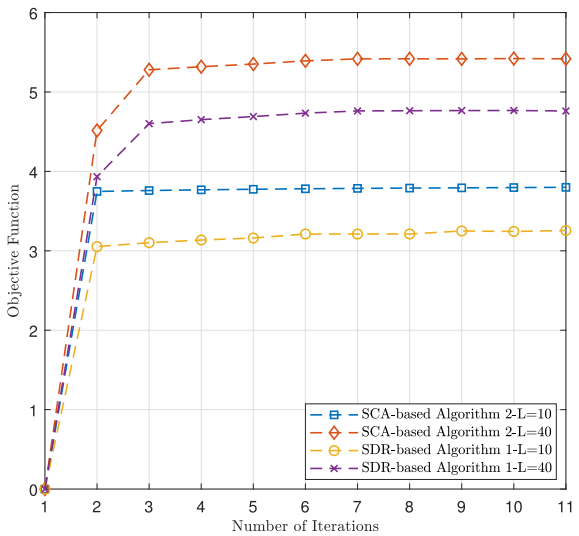

FIGURE 5. Convergence of Algorithm 1 and Algorithm 2 for different IRS elements.

our proposed methods in achieving near-optimal solutions for the hybrid active/passive IRS-aided WPCN, facilitating improved network performance and throughput fairness.

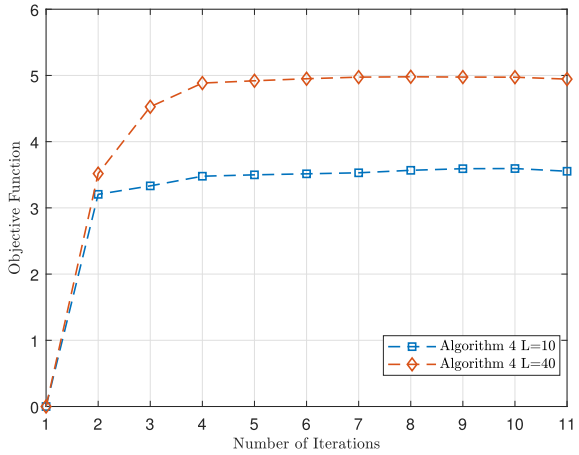

FIGURE 6. Convergence of Algorithm 4 for different IRS elements.

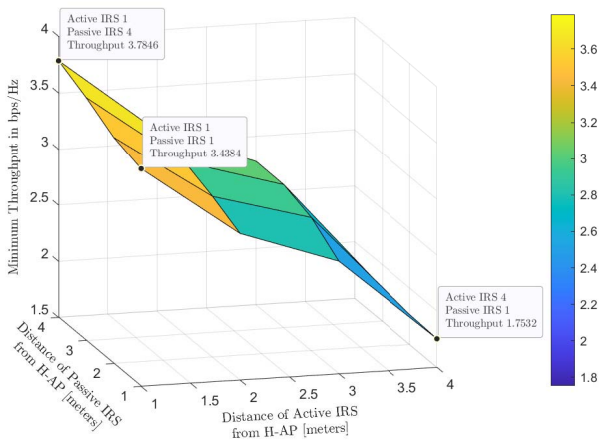

FIGURE 7. Minimum throughput versus Active and Passive IRS locations from the H-AP.

Fig. 7 illustrates the impact of the locations of both active and passive IRSs from the H-AP. Our findings reveal that the placement of the passive IRS has a negligible effect on the minimum throughput. In contrast, as the active IRS is positioned farther from the H-AP, a substantial decrease in minimum throughput is observed. The results highlight a significant distinction in the influence of location between passive and active IRSs. While the passive IRS, with its reflective properties, demonstrates a consistent minimum throughput across various locations, the active IRS, due to its ability to actively amplify signals, exhibits a more pronounced impact on throughput as its distance from the H-AP increases. This is because the active IRS located near the H-AP can actively amplify the incident signals, compensating for the propagation loss and enhancing the received signal power at the H-AP. As the active IRS is positioned farther and farther away from the H-AP, the system's performance gradually degrades. This is because, at longer distances, the amplification effect becomes weaker, and the cascaded path loss between the H-AP and the active IRS increases, diminishing the benefits of the active IRS.

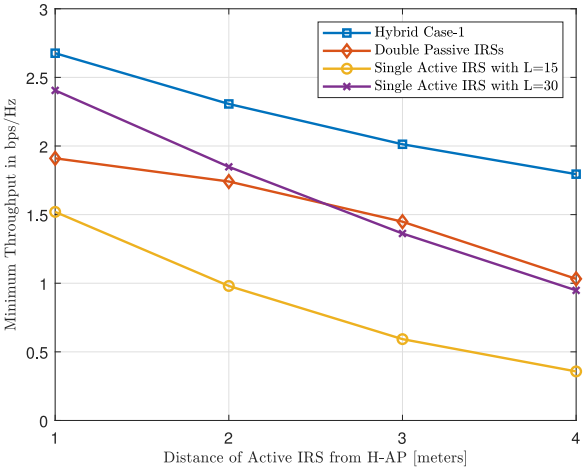

FIGURE 8. Minimum throughput versus increased distances of Active IRS from the H-AP.

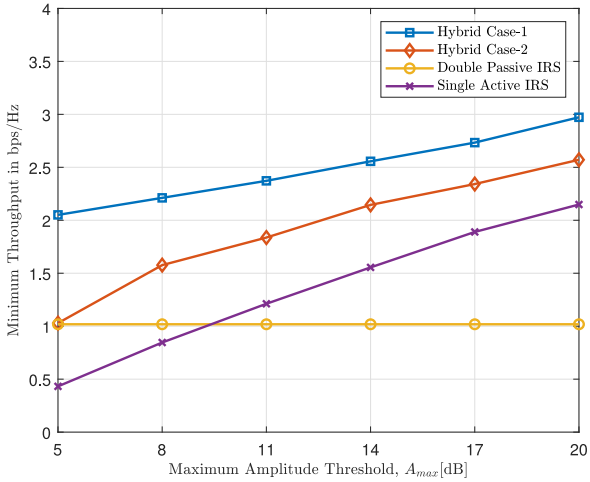

FIGURE 9. Minimum throughput versus the increasing maximum amplitude limit.

Furthermore, Fig. 8 shows the effect of the active IRS's location from the hybrid access point in *Hybrid Case-1* and double passive IRS schemes, where reflecting elements L_1 and L_2 are both set to 15. Additionally, we consider two cases for the single active IRS scheme with reflecting elements $L = 15$ and $L = 30$. The results indicate that the hybrid system achieves higher throughput when the active IRS is placed closer to the H-AP. We compare the performance of our proposed algorithm with the double passive IRSs and the single active IRS schemes. The results consistently show that our proposed algorithm outperforms the other schemes, demonstrating its effectiveness in achieving better network performance and throughput enhancement. An interesting observation is that the single active IRS with $L = 15$ has lower performance compared to the double passive IRSs. This is because, at a shorter distance, the double passive IRSs can provide strong multi-reflection paths, compensating for the lack of active amplification. However, when the reflecting elements of the single active IRS is increased to $L = 30$, its performance surpasses that of the double passive IRSs when placed closer to the H-AP. This is due to the stronger active amplification effect with the larger number of reflecting elements, which helps overcome the multi-path reflection advantage of the double passive IRSs.

Nonetheless, as the active IRS moves even farther away from the H-AP, its performance starts to degrade compared to the double passive IRS. This is because, at such long distances, the limitations of active amplification and the increased cascaded path loss outweigh the benefits of the single active IRS, making the double passive IRS scheme more effective. In contrast, the proposed hybrid approach capitalizes on the active and multi-reflection effects, achieving better overall performance regardless of the active IRS's location. The combination of active and passive IRS elements enables the system to adapt to various scenarios, and optimizes the network's performance, making the hybrid approach the most favorable choice for practical deployment in WPCNs.

Fig. 9 illustrates a comprehensive comparison of minimum throughput with respect to the active IRS's maximum amplitude limit, denoted as A_{max}, of the incident signal. The analysis assumes a uniform amplitude limit for both downlink and uplink transmissions, i.e., $\alpha_{l,max} = \beta_{l,max} = A_{max}$ for all links l. The results clearly show that increasing A_{max} leads to a corresponding increase in the minimum throughput. This is due to the active IRS's ability to provide enhanced amplification gain, compensating for signal attenuation, and improving the received signal power at the devices. In addition to the impact of A_{max}, the deployment of the active IRS also significantly influences the system's performance. Notably, *Hybrid Case-1* where the active IRS is placed near the H-AP, consistently outperforms *Hybrid Case-1* where the active IRS is placed near the devices. The reason is that when the active IRS is located close to the receiver, it effectively amplifies the attenuated signals, leading to stronger signals reaching the receiver.

Moreover, joint deployment of active and passive IRSs in the proposed hybrid system yields superior performance compared to both single and double passive IRS configurations. This is due to the complementary effects of the active IRS's amplification and the multiple IRSs' multi-reflection effects. The active IRS enhances the signal power, while the multiple IRSs provide multiple reflected signals, resulting in improved overall performance. Interestingly, we also notice that the single active IRS scheme performs better than the double passive IRS scheme when maximum amplitude limit A_{max} is higher. This is because the single active IRS can leverage its higher amplification power to overcome the double path loss effects observed in the double passive IRS configuration.

Fig. 10 examines total downlink energy harvesting as a function of maximum amplitude limit A_{max}. As expected, the total energy harvesting increases as A_{max} increases. This highlights the significant energy harvesting benefits provided by the active IRS, which amplifies the incident

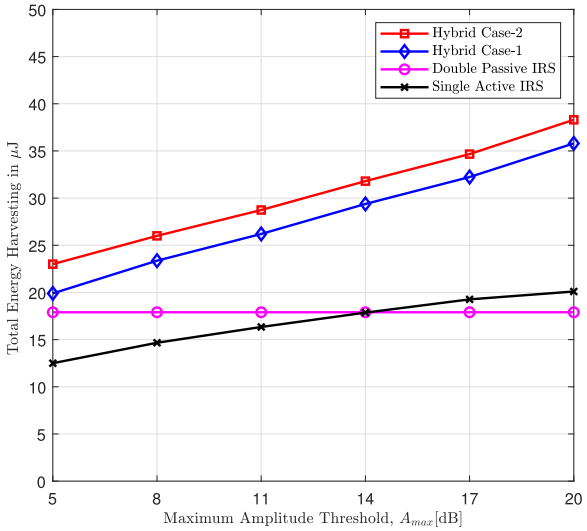

FIGURE 10. Total energy harvesting versus the increasing maximum amplitude limit.

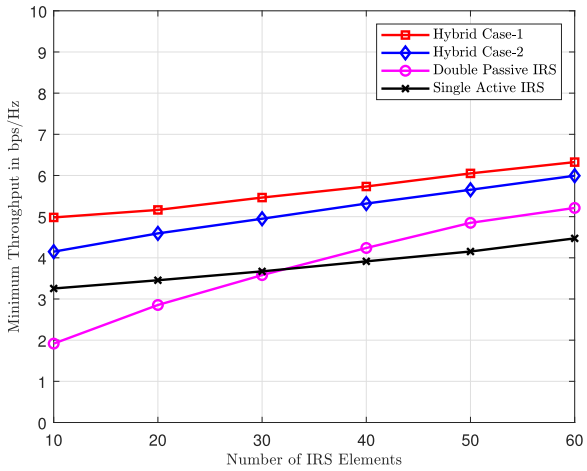

FIGURE 11. Minimum throughput versus the number of IRS elements.

signals and improves the energy capture capability of the wireless-powered devices.

Fig. 11 displays the minimum throughput plotted against the number of intelligent reflecting surface elements, represented as $L = L_1 + L_2$, in various deployment designs. As expected, the sum rate shows an increasing trend with a larger number of IRS elements, indicating the potential of IRS-assisted systems to enhance overall network performance. Remarkably, the proposed algorithm exhibits significant improvements in the minimum rate experienced by devices. The algorithm effectively leverages the benefits of intelligent reflecting surfaces, resulting in substantial throughput enhancements, and ensuring a more equitable user experience across the network. These promising results underscore the efficacy of the proposed approach for optimizing throughput in 6G wireless-powered communications networks.

Figure 12 shows an analysis involving amplified thermal noise and its impact on the average achievable throughput in the uplink. Our findings revealed a notable trend: as

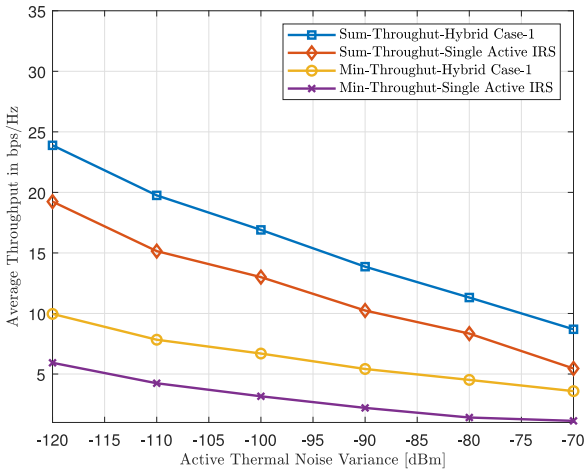

FIGURE 12. Impact of amplified thermal noise on the average achievable throughput.

amplified thermal noise increases, the achievable throughput decreases. This observation shows a critical limitation associated with active IRS elements. While increasing active elements can potentially boost throughput, it also leads to amplified thermal noise, posing challenges in striking a balance between maximizing received signal power and minimizing noise in the uplink. Despite these challenges, our study demonstrated that our proposed hybrid architecture outperforms a single active IRS in this context. This comparison demonstrates the superiority of our hybrid approach in managing the trade-offs between maximizing signal power and mitigating amplified thermal noise, ultimately resulting in improved performance in the uplink scenario.

Figure 13 shows the sum throughput under specific conditions: $K = 2$, $d_1 = 2m$, and $d_2 = 4m$, while varying the number of elements in the IRSs, denoted as $L = L_1 + L_2$. The data is obtained through averaging over 100 randomly generated channel realizations. An interesting observation arises from comparing the two hybrid cases, *Hybrid Case-1* and *Hybrid Case-1*. Notably, *Hybrid Case-1* demonstrates superior performance compared to *Hybrid Case-1*. Furthermore, For the *Hybrid Case-1*, the far user experiences higher throughput in comparison with the *Hybrid Case-1*. This particular outcome highlights the effectiveness of placing active IRS elements closer to the H-AP. This observation underscores the significance of the IRS's placement concerning the H-AP, where the strategic deployment of active IRS elements near the H-AP yields improved throughput fairness, especially for users situated at greater distances.

Fig. 14 presents the feasibility analysis of our proposed algorithm for different numbers of IRS elements, compared with the random allocation of resources approach. In the random allocation of resources approach, we randomly select phases and amplitudes for the active and passive beams, and we distribute time resources by equally dividing them into $K+1$ time slots. Simulations are conducted for 100 randomly distributed channels. The results show that our proposed

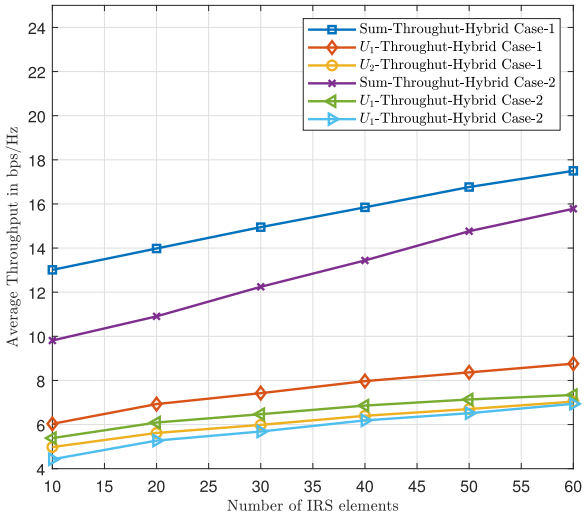

FIGURE 13. Average throughput versus the number of IRS elements.

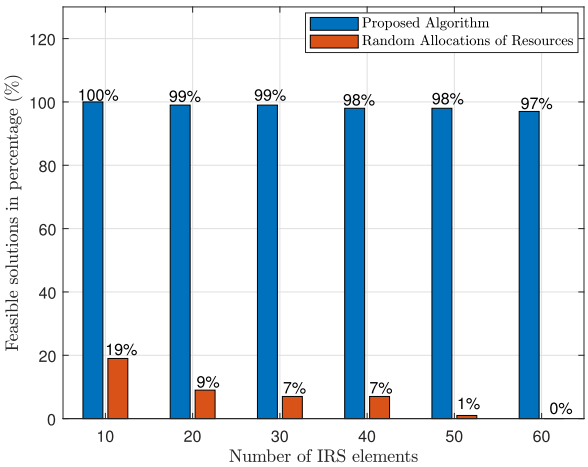

FIGURE 14. Feasibility analysis for the proposed algorithm and random allocations of resources versus number of IRS reflecting elements.

algorithm achieves maximum feasibility compared to the random allocation of resources. Conversely, the scheme using random IRS phase shifts yields significantly fewer feasible solutions, even below 20%. This limitation arises because random phase shift allocation fails to ensure alignment between IRS beams on the uplink and downlink with the communication channels, resulting in suboptimal network performance.

Additionally, we observe that the in-feasibility of solutions increases with the growing number of elements. This challenge is attributed to the increased complexity of designing an optimal solution as the number of elements rises. Therefore, this emphasizes the significance of optimizing IRS passive beamforming on both the uplink and downlink to enhance network performance.

VI. CONCLUSION

This paper presents a hybrid, active and passive IRS-based framework to enhance throughput fairness in wireless powered communication networks. We addressed the challenge of the doubly-near-far problem where nearby devices with better channel conditions experience higher energy harvesting and throughput compared to devices at a distance. The cascaded channel path loss in networks with multiple IRSs exacerbates this issue. To tackle this, we formulated a throughput fairness optimization problem, jointly optimizing active and passive beamforming and time allocations for both uplink and downlink, aiming to maximize the minimum throughput among devices. Through extensive simulations and numerical analysis, we demonstrated the superiority of our proposed framework over alternative configurations, such as systems employing a single active IRS or the conventional double passive IRS. The results showed that our hybrid approach significantly improves network performance and throughput fairness, making it a compelling choice for practical WPCN deployments. To efficiently solve the non-convex optimization problem, we decomposed the optimization problem into three sub-problems and iteratively solved them. This approach, along with sophisticated techniques such as semi-definite relaxation, successive convex approximation, and the Lagrangian method, facilitated convergence of the optimization process and the achievement of near-optimal solutions. Overall, our hybrid active/passive IRS-based framework has the potential to revolutionize WPCNs, addressing the challenges of throughput fairness and offering enhanced network performance. As the demand for wireless power and communication technologies continues to grow, our proposed approach represents a promising step towards more efficient and equitable wireless networks in the future.

APPENDIX A

By taking the partial derivative of $\mathcal{L}(\eta, t_0, t_k, \mu, \chi_k, \vartheta_k)$ with respect to t_0 and t_k, respectively, we have

$$\frac{\partial \mathcal{L}}{\partial t_0} = \sum_{k=1}^{K} \frac{\chi_k M_k}{1 + M_k \frac{t_0}{t_k}} - \mu - \sum_{k=1}^{K} \vartheta_k \tag{35}$$

$$\frac{\partial \mathcal{L}}{\partial t_k} = \chi_k \left[\log_2\left(1 + M_k \frac{t_0}{t_k}\right) - \frac{M_k \frac{t_0}{t_k}}{1 + M_k \frac{t_0}{t_k}} \right] - \mu + \vartheta_k N_k, \quad \forall k \tag{36}$$

$$\frac{\partial \mathcal{L}}{\partial \mu} = 1 - \sum_{j=0}^{K} t_j \tag{37}$$

$$\frac{\partial \mathcal{L}}{\partial \vartheta_k} = \vartheta_k N_k - t_0, \quad \forall k \tag{38}$$

Based on KKT conditions the closed form solution of t_0^* and t_k^*, can be obtained by $\frac{\partial \mathcal{L}}{\partial t_0} = 0$, and $\frac{\partial \mathcal{L}}{\partial t_k} = 0$, respectively.

$$\sum_{k=1}^{K} \frac{\chi_k M_k}{1 + M_k \frac{t_0^*}{t_k^*}} = \mu + \sum_{k=1}^{K} \vartheta_k \tag{39}$$

$$\log_2\left(1 + M_k \frac{t_0^*}{t_k^*}\right) - \frac{M_k \frac{t_0^*}{t_k^*}}{1 + M_k \frac{t_0^*}{t_k^*}} = \frac{\mu - \vartheta_k N_k}{\chi_k}, \quad \forall k \tag{40}$$

By solving Eq. (40), we can find an optimal solution of $\Lambda_k^* = \frac{t_k^*}{t_0^*}$ which also satisfies the Eq. (39) for given $\mu, \boldsymbol{\chi}, \boldsymbol{\vartheta}$, otherwise we update $\mu, \boldsymbol{\chi}, \boldsymbol{\vartheta}$ using Eqs. (30)-(32) until feasibility met.

Moreover, by $\frac{\partial \mathcal{L}}{\partial \mu} = 0$, we get

$$1 - t_0^* = \sum_{k=1}^{K} t_k^* \tag{41}$$

And, with the optimal solution of (39) and (40), Λ_k^*, we have $t_k^* = \Lambda_k^* t_0^*$. Hence using (41), we can derive (28) and (29).

APPENDIX B

Here, we will show the problem formulation and solution For *Hybrid Case-2*. However, we omit the detailed explanation and expressions to avoid repetitions of content or straightforward implementations. In Fig. 1, we consider IRS-1 consists of L_1 passive elements and IRS-2 consists of L_2 active elements. We can reproduce the Eq. (1) and Eq. (5) for the *Hybrid Case-2* as follows

$$y_k = \sqrt{P_t}\Big(h_{2,k}^H \Gamma_{2,d} G^H \Gamma_{1,d} g_1 + h_{2,k}^H \Gamma_{2,d} g_2 + h_{1,k}^H \Gamma_{1,d} g_1\Big) x_0 + h_{2,k}^H \Gamma_{2,d} z_{IRS} + z_k, \quad \forall k, \tag{42a}$$

$$r_k = \sqrt{p_k}\Big(g_1^H \Gamma_{1,u} G \Gamma_{2,u} h_{2,k} + g_2^H \Gamma_{2,u} h_{2,k} + g_1^H \Gamma_{1,u} h_{1,k}\Big) x_k + \Big(g_1^H \Gamma_{1,u} G \Gamma_{2,u} + g_2^H \Gamma_{2,u}\Big) z_{IRS} + z_A, \quad \forall k, \tag{43a}$$

Now, $\Gamma_{i,d} = \text{diag}\{\alpha_{i,1} e^{j\theta_{i,1}}, \alpha_{i,2} e^{j\theta_{i,2}}, \ldots, \alpha_{i,L_i} e^{j\theta_{i,L_i}}\}$ for $i \in [1,2]$ with $\alpha_{1,l} \in [0,1]$ and $\alpha_{2,l} \in [0, \alpha_{l,max}]$, $\alpha_{l,max} \geq 1$. And $\Gamma_{i,u} = \text{diag}\{\beta_{i,1} e^{j\omega_{i,1}}, \beta_{i,2} e^{j\omega_{i,2}}, \ldots, \beta_{i,L_i} e^{j\omega_{i,L_i}}\}$ for $i \in [1,2]$ with $\beta_{1,l} \in [0,1]$, and $\beta_{2,l} \in [0, \beta_{l,max}]$, $\beta_{l,max} \geq 1$. By using definitions of $\{\mathbf{v}_d, \mathbf{w}_d, \mathbf{v}_u, \mathbf{w}_u\}$ from *Proposition 1* and *Proposition 2* we will reproduce the $\mathcal{P}1$ for the *Hybrid Case-2* as follows

$$\mathcal{P}2 \max_{t_0, \{t_k\}, \mathbf{v}_d, \mathbf{w}_d, \mathbf{v}_u, \mathbf{w}_u} \min_k R_k(p_k, t_k, v_u, w_u) \tag{44a}$$

$$\text{s.t.} \quad |[\mathbf{v}_d]_l| \leq= 1, \quad l = 1, 2, 3, \cdots L_1 \tag{44b}$$

$$|[\mathbf{w}_d]_l| \leq \alpha_{l,max}, \quad l = 1, 2, 3, \ldots L_2 \tag{44c}$$

$$|[\mathbf{v}_u]_l| = 1, \quad l = 1, 2, 3, \ldots L_1, \tag{44d}$$

$$|[\mathbf{w}_u]_l| \leq \beta_{l,max}, \quad l = 1, 2, 3, \ldots L_2 \tag{44e}$$

$$(8b), \ (8c), \ (8h) \tag{44f}$$

Next, we can solve $\mathcal{P}2$ using the proposed approach discussed in Section III.

REFERENCES

[1] F. Guo, F. R. Yu, H. Zhang, X. Li, H. Ji, and V. C. M. Leung, "Enabling massive IoT toward 6G: A comprehensive survey," *IEEE Internet Things J.*, vol. 8, no. 15, pp. 11891–11915, Aug. 2021.

[2] X. Li, Z. Xie, Z. Chu, V. G. Menon, S. Mumtaz, and J. Zhang, "Exploiting benefits of IRS in wireless powered NOMA networks," *IEEE Trans. Green Commun. Netw.*, vol. 6, no. 1, pp. 175–186, Mar. 2022.

[3] S. Verma, S. Kaur, M. A. Khan, and P. S. Sehdev, "Toward green communication in 6G-enabled massive Internet of Things," *IEEE Internet Things J.*, vol. 8, no. 7, pp. 5408–5415, Apr. 2021.

[4] X. Liu, Z. Qin, Y. Gao, and J. A. McCann, "Resource allocation in wireless powered IoT networks," *IEEE Internet Things J.*, vol. 6, no. 3, pp. 4935–4945, Jun. 2019.

[5] X. Li, C. Zhang, C. He, G. Chen, and J. A. Chambers, "Sum-rate maximization in IRS-assisted wireless power communication networks," *IEEE Internet Things J.*, vol. 8, no. 19, pp. 14959–14970, Oct. 2021.

[6] H. Ju and R. Zhang, "Throughput maximization in wireless powered communication networks," *IEEE Trans. Wireless Commun.*, vol. 13, no. 1, pp. 418–428, Jan. 2014.

[7] S. Bi, C. K. Ho, and R. Zhang, "Wireless powered communication: Opportunities and challenges," *IEEE Commun. Mag.*, vol. 53, no. 4, pp. 117–125, Apr. 2015.

[8] W. Shi, Q. Wu, F. Xiao, F. Shu, and J. Wang, "Secrecy throughput maximization for IRS-aided MIMO wireless powered communication networks," *IEEE Trans. Commun.*, vol. 70, no. 11, pp. 7520–7535, Nov. 2022.

[9] Q. Wu and R. Zhang, "Towards smart and reconfigurable environment: Intelligent reflecting surface aided wireless network," *IEEE Commun. Mag.*, vol. 58, no. 1, pp. 106–112, Jan. 2020.

[10] E. Basar, M. Di Renzo, J. De Rosny, M. Debbah, M.-S. Alouini, and R. Zhang, "Wireless communications through reconfigurable intelligent surfaces," *IEEE Access*, vol. 7, pp. 116753–116773, 2019.

[11] S. Kisseleff, W. A. Martins, H. Al-Hraishawi, S. Chatzinotas, and B. Ottersten, "Reconfigurable intelligent surfaces for smart cities: Research challenges and opportunities," *IEEE Open J. Commun. Soc.*, vol. 1, pp. 1781–1797, 2020.

[12] Q. Wu and R. Zhang, "Intelligent reflecting surface enhanced wireless network via joint active and passive beamforming," *IEEE Trans. Wireless Commun.*, vol. 18, no. 11, pp. 5394–5409, Nov. 2019.

[13] I. Hameed, M. R. Camana, P. V. Tuan, and I. Koo, "Intelligent reflecting surfaces for sum-rate maximization in cognitive radio enabled wireless powered communication network," *IEEE Access*, vol. 11, pp. 16021–16031, 2023.

[14] F. Fang, Y. Xu, Q.-V. Pham, and Z. Ding, "Energy-efficient design of IRS-NOMA networks," *IEEE Trans. Veh. Technol.*, vol. 69, no. 11, pp. 14088–14092, Nov. 2020.

[15] Q. Wu, S. Zhang, B. Zheng, C. You, and R. Zhang, "Intelligent reflecting surface-aided wireless communications: A tutorial," *IEEE Trans. Commun.*, vol. 69, no. 5, pp. 3313–3351, May 2021.

[16] M. Diamanti, E. E. Tsiropoulou, and S. Papavassiliou, "The joint power of NOMA and reconfigurable intelligent surfaces in SWIPT networks," in *Proc. IEEE 22nd Int. Workshop Signal Process. Adv. Wireless Commun. (SPAWC)*, 2021, pp. 621–625.

[17] T. J. Cui, M. Q. Qi, X. Wan, J. Zhao, and Q. Cheng, "Coding metamaterials, digital metamaterials and programmable metamaterials," *Light Sci. Appl.*, vol. 3, no. 10, p. e218, Oct. 2014. [Online]. Available: https://doi.org/10.1038/lsa.2014.99

[18] Y. Zheng, S. Bi, Y. J. Zhang, Z. Quan, and H. Wang, "Intelligent reflecting surface enhanced user cooperation in wireless powered communication networks," *IEEE Wireless Commun. Lett.*, vol. 9, no. 6, pp. 901–905, Jun. 2020.

[19] H. Cao, Z. Li, and W. Chen, "Resource allocation for IRS-assisted wireless powered communication networks," *IEEE Wireless Commun. Lett.*, vol. 10, no. 11, pp. 2450–2454, Nov. 2021.

[20] W. Mei, B. Zheng, C. You, and R. Zhang, "Intelligent reflecting surface-aided wireless networks: From single-reflection to multireflection design and optimization," *Proc. IEEE*, vol. 110, no. 9, pp. 1380–1400, Sep. 2022.

[21] C. You, B. Zheng, W. Mei, and R. Zhang, "How to deploy intelligent reflecting surfaces in wireless network: BS-side,user-side, or both sides?" *J. Commun. Inf. Netw.*, vol. 7, no. 1, pp. 1–10, Mar. 2022. [Online]. Available: http://www.infocomm-journal.com/jcin/EN/abstract/article_172231.shtml

[22] Y. Han, S. Zhang, L. Duan, and R. Zhang, "Cooperative double-IRS aided communication: Beamforming design and power scaling," *IEEE Wireless Commun. Lett.*, vol. 9, no. 8, pp. 1206–1210, Aug. 2020.

[23] B. Zheng, C. You, and R. Zhang, "Double-IRS assisted multi-user MIMO: Cooperative passive beamforming design," *IEEE Trans. Wireless Commun.*, vol. 20, no. 7, pp. 4513–4526, Jul. 2021.

[24] Y. Han, S. Zhang, L. Duan, and R. Zhang, "Double-IRS aided MIMO communication under LoS channels: Capacity maximization and scaling," *IEEE Trans. Commun.*, vol. 70, no. 4, pp. 2820–2837, Apr. 2022.
[25] Y. Li, C. You, and Y. J. Chun, "Active-IRS aided wireless network: System modeling and performance analysis," *IEEE Commun. Lett.*, vol. 27, no. 2, pp. 487–491, Feb. 2023.
[26] Z. Kang, C. You, and R. Zhang, "Active-IRS-aided wireless communication: Fundamentals, designs and open issues," 2023, *arXiv:2301.04311*.
[27] Z. Zhang et al., "Active RIS vs. passive RIS: Which will prevail in 6G?" *IEEE Trans. Commun.*, vol. 71, no. 3, pp. 1707–1725, Mar. 2023.
[28] G. Chen, Q. Wu, C. He, W. Chen, J. Tang, and S. Jin, "Active IRS aided multiple access for energy-constrained IoT systems," *IEEE Trans. Wireless Commun.*, vol. 22, no. 3, pp. 1677–1694, Mar. 2023.
[29] P. Zeng, D. Qiao, Q. Wu, and Y. Wu, "Throughput maximization for active intelligent reflecting surface-aided wireless powered communications," *IEEE Wireless Commun. Lett.*, vol. 11, no. 5, pp. 992–996, May 2022.
[30] L. Dong, H.-M. Wang, and J. Bai, "Active reconfigurable intelligent surface aided secure transmission," *IEEE Trans. Veh. Technol.*, vol. 71, no. 2, pp. 2181–2186, Feb. 2022.
[31] S. Zargari, A. Hakimi, C. Tellambura, and S. Herath, "Multiuser MISO PS-SWIPT systems: Active or passive RIS?" *IEEE Wireless Commun. Lett.*, vol. 11, no. 9, pp. 1920–1924, Sep. 2022.
[32] H. Niu et al., "Active RIS-assisted secure transmission for cognitive satellite terrestrial networks," *IEEE Trans. Veh. Technol.*, vol. 72, no. 2, pp. 2609–2614, Feb. 2023.
[33] R. Long, Y.-C. Liang, Y. Pei, and E. G. Larsson, "Active reconfigurable intelligent surface-aided wireless communications," *IEEE Trans. Wireless Commun.*, vol. 20, no. 8, pp. 4962–4975, Aug. 2021.
[34] K. Zhi, C. Pan, H. Ren, K. K. Chai, and M. Elkashlan, "Active RIS versus passive RIS: Which is superior with the same power budget?" *IEEE Commun. Lett.*, vol. 26, no. 5, pp. 1150–1154, May 2022.
[35] I. Hameed and I. Koo, "Exploiting active-IRS by Maximizing throughput in wireless powered communication networks," in *Proc. 19th Adv. Intell. Comput. Technol. Appl.*, 2023, pp. 367–376.
[36] C. You and R. Zhang, "Wireless communication aided by intelligent reflecting surface: Active or passive?" *IEEE Wireless Commun. Lett.*, vol. 10, no. 12, pp. 2659–2663, Dec. 2021.
[37] R. Dong et al., "Joint beamforming and phase shift design for hybrid-IRS-and-UAV-aided directional modulation network," 2023, *arXiv:2304.11514*.
[38] N. T. Nguyen, Q.-D. Vu, K. Lee, and M. Juntti, "Hybrid relay-reflecting intelligent surface-assisted wireless communications," *IEEE Trans. Veh. Technol.*, vol. 71, no. 6, pp. 6228–6244, Jun. 2022.
[39] Q. Peng, Q. Wu, G. Chen, R. Liu, S. Ma, and W. Chen, "Hybrid active-passive IRS assisted energy-efficient wireless communication," *IEEE Commun. Lett.*, vol. 27, no. 8, pp. 2202–2206, Aug. 2023.
[40] M. Fu and R. Zhang, "Active and passive IRS jointly aided communication: Deployment design and achievable rate," *IEEE Wireless Commun. Lett.*, vol. 12, no. 2, pp. 302–306, Feb. 2023.
[41] B. Lyu, D. T. Hoang, S. Gong, and Z. Yang, "Intelligent reflecting surface assisted wireless powered communication networks," in *Proc. IEEE Wireless Commun. Netw. Conf. Workshops (WCNCW)*, 2020, pp. 1–6.
[42] Z. Li, W. Chen, Q. Wu, H. Cao, K. Wang, and J. Li, "Robust beamforming design and time allocation for IRS-assisted wireless powered communication networks," *IEEE Trans. Commun.*, vol. 70, no. 4, pp. 2838–2852, Apr. 2022.
[43] B. Lyu, P. Ramezani, D. T. Hoang, and A. Jamalipour, "IRS-assisted downlink and uplink NOMA in wireless powered communication networks," *IEEE Trans. Veh. Technol.*, vol. 71, no. 1, pp. 1083–1088, Jan. 2022.
[44] L. Cantos and Y. H. Kim, "IRS assisted wireless powered communication: Active or passive?" in *Proc. 13th Int. Conf. Inf. Commun. Technol. Converg. (ICTC)*, 2022, pp. 184–186.
[45] M. Fu, W. Mei, and R. Zhang, "Multi-active/passive-IRS enabled wireless information and power transfer: Active IRS deployment and performance analysis," *IEEE Commun. Lett.*, vol. 27, no. 8, pp. 2217–2221, Aug. 2023.
[46] Z. Wang, L. Liu, and S. Cui, "Channel estimation for intelligent reflecting surface assisted multiuser communications: Framework, algorithms, and analysis," *IEEE Trans. Wireless Commun.*, vol. 19, no. 10, pp. 6607–6620, Oct. 2020.
[47] H. Guo and V. K. N. Lau, "Uplink cascaded channel estimation for intelligent reflecting surface assisted multiuser MISO systems," *IEEE Trans. Signal Process.*, vol. 70, pp. 3964–3977, Jul. 2022, doi: 10.1109/TSP.2022.3193626.
[48] B. Zheng, C. You, and R. Zhang, "Efficient channel estimation for double-IRS aided multi-user MIMO system," *IEEE Trans. Commun.*, vol. 69, no. 6, pp. 3818–3832, Jun. 2021.
[49] M. Grant and S. Boyd. "CVX: Matlab software for disciplined convex programming, version 2.1." Mar. 2014. [Online]. Available: http://cvxr.com/cvx
[50] O. Mehanna, K. Huang, B. Gopalakrishnan, A. Konar, and N. D. Sidiropoulos, "Feasible point pursuit and successive approximation of non-convex QCQPs," *IEEE Signal Process. Lett.*, vol. 22, no. 7, pp. 804–808, Jul. 2015.
[51] A. A. Nasir, H. D. Tuan, T. Q. Duong, and H. V. Poor, "Secrecy rate beamforming for multicell networks with information and energy harvesting," *IEEE Trans. Signal Process.*, vol. 65, no. 3, pp. 677–689, Feb. 2017.
[52] S. Boyd and L. Vandenberghe, *Convex Optimization*. Cambridge, U.K.: Cambridge Univ. Press, 2004.
[53] E. Karipidis, N. D. Sidiropoulos, and Z.-Q. Luo, "Far-field multicast beamforming for uniform linear antenna arrays," *IEEE Trans. Signal Process.*, vol. 55, no. 10, pp. 4916–4927, Oct. 2007.

IQRA HAMEED received the B.E. and M.E. degrees in electrical engineering from University of Engineering and Technology, Lahore, Pakistan in 2013 and 2017, respectively. She is currently pursuing the Ph.D. degree with the School of Electrical, Electronic and Computer Engineering, University of Ulsan, Ulsan, South Korea. Her research interests include wireless powered communication networks, deep learning, and optimizations.

INSOO KOO (Member, IEEE) received the B.E. degree from Konkuk University, Seoul, South Korea, in 1996, and the M.Sc. and Ph.D. degrees from the Gwangju Institute of Science and Technology, Gwangju, South Korea, in 1998 and 2002, respectively, where he was a Research Professor with Ultrafast FiberOptic Networks Research Center from 2002 to 2004. In 2003, he was a Visiting Scholar with the Royal Institute of Science and Technology, Stockholm, Sweden. In 2005, he joined the University of Ulsan, Ulsan, South Korea, where he is currently a Full Professor. His current research interests include spectrum sensing issues for CRNs, channel and power allocation for cognitive radios and military networks, SWIPT MIMO issues for CRs, MAC, and routing protocol design for UW-ASNs, and relay selection issues in CCRNs.